Scattered Pilot-Based Channel Estimation for Channel Adaptive FBMC-OQAM Systems

Martin Fuhrwerk, Sanam Moghaddamnia and Jürgen Peissig

***Abstract*—Shaping the pulse of FilterBank MultiCarrier with Offset Quadrature Amplitude Modulation subcarrier modulation (FBMC-OQAM) systems offers a new degree of freedom for the design of mobile communication systems. In previous studies, we evaluated the gains arising from the application of Prototype Filter Functions (PFFs) and subcarrier spacing matched to the delay and Doppler spreads of doubly dispersive channels. In this paper, we investigate the impact of having imperfect channel knowledge at the receiver on the performance of Channel Adaptive Modulation (CAM) in terms of channel estimation errors and Bit Error Rate (BER). To this end, the channel estimation error for two different interference mitigation schemes proposed in the literature is derived analytically and its influence on the BER performance is analyzed for practical channel scenarios. The results show that FBMC-OQAM systems utilizing CAM and scattered pilot-based channel estimation provide a significant performance gain compared with the current one system design for a variety of channel scenarios ("one-fits-all") approach. Additionally, we verified that the often used assumption of a flat channel in the direct neighborhood of a pilot symbol is not valid for practical scenarios.**

***Index Terms*—FBMC, channel adaptive systems, offset-QAM-OFDM / FBMC-OQAM, channel estimation, intrinsic interference, interference mitigation, scattered pilots**

I. Introduction

NOWADAYS, multicarrier systems based on Cyclic Prefix-Orthogonal Frequency-Division Multiplexing (CP-OFDM), e.g. Long-Term Evolution (LTE), Digital Video Broadcasting - Terrestrial (DVB-T) and Wireless Local Area Networks (WLANs), have been designed to provide an optimal trade-off between spectral efficiency and high Quality of Service (QoS) over a wide range of different channel scenarios. For future mobile communication systems, this "one-fits-all" approach no longer is favored [1], as its performance in terms of capacity degrades considerably if the system is not operating in one of the target channel scenarios. The reason for this is the limited channel adaptability available in currently deployed mobile communication systems, e.g. adaptive modulation and coding schemes in LTE [2] and its successors LTE Advanced and LTE Advanced Pro.

One approach to avoid the arising data rate loss is the utilization of a modulation scheme with the capability of Channel Adaptive Pulse Shaping (CAPS). This has been proven to maximize the system capacity for a given symbol duration and subcarrier configuration [3]. Similar to CP-OFDM, windowed OFDM, Filtered MultiTone (FMT) and Universal-Filtered MultiCarrier (UFMC) [4] schemes also suffer from spectral efficiency loss due to the usage of an undersampled time-frequency lattice grid. Thus Staggered MultiTone (SMT) schemes like FBMC-OQAM, which utilize a critically sampled lattice grid [5], have been proposed for future wireless communication systems, e.g. 5th Generation (5G) cellular radio [6], [7]. In contrast to CP-OFDM, FBMC-OQAM allows the usage of arbitrary pulse shapes, which enables optimal adaptation of a transmission system to the actual channel conditions, thus preserving the maximum available channel capacity. Additionally, utilizing proper pulse shapes allows to reduce side lobes significantly and thus improves the coexistence capabilities of mobile communication systems with adjacent or in-band interferers [8].

In [9], [10] and related publications it has been shown that the application of an FBMC-OQAM modulation scheme can outperform CP-OFDM in terms of BER and spectral efficiency without considering potential gains provided by CAPS. Theoretical investigations into the impact of doubly dispersive channels on the performance of FBMC systems have been carried out in [11], confirming that lattice grid optimization can provide an increased robustness against Inter-Symbol Interference (ISI) and Inter-Carrier Interference (ICI) compared to state-of-the-art OFDM systems. For preamble based channel estimation, a channel adaptive pulse shape design has been proposed to provide significant gains in terms of channel estimation and BER performance [12]. Utilizing a generic channel model, [13] provides a quantitative investigation of the gains achievable by the application of CAPS to an FBMC-OQAM system operating in doubly dispersive channels. It is shown that CAPS can provide a Signal-to-Interference Ratio (SIR) improvement of approximately 3 to 4 dB at the receiver Analysis FilterBank (AFB). In [14] the performance of the Isotropic

M. Fuhrwerk, S. Moghaddamnia and J. Peissig are with Leibniz Universität Hannover e-mail: fuhrwerk@ikt.uni-hannover.de.

Manuscript received June 09, 2016; revised September 13, 2016, November 29, 2016.

Orthogonal Transform Algorithm (IOTA) PFF based on Extended Gaussian Functions (EGF) for two specific dispersive channels is compared to CP-OFDM. Both [13] and [14] show that pulse shape adaptation based on the actual channel state information can indeed improve the system performance in FBMC based systems. In [15] we investigate the quantitative performance gains that can be achieved by utilizing FBMC-OQAM with CAPS utilizing an LTE like system operating in COST 207 channels [16] and compared the results to a CP-OFDM based system. We showed that FBMC-OQAM systems with a suitable PFF can outperform the classical CP-OFDM scheme in terms of BER and throughput.

However, to prevent increased latency or out-of-band emission, the PFF applied for CAPS cannot be spread arbitrarily in time or frequency domain and thus the performance gains achieved by CAPS are limited. Therefore, we propose a novel system design paradigm [17], which utilizes a cell and/or user specific Channel Adaptive Subcarrier Spacing (CASS), as depicted in Figure 1. This enables the optimal adaption of a transmission system to a certain channel environment. From implementation point of view, it is not beneficial to utilize arbitrary symbol durations within a single system design, as this significantly increases system complexity and costs. Therefore, we propose a system design which combines CAPS and CASS to a unified scheme referred to as CAM.

Our previous investigations regarding CAM based on the assumption of perfect channel knowledge at the receiver side and utilizing a Zero Forcing (ZF) equalizer [13], [15]. In this work, we investigate the influence of imperfect channel estimation based on scattered pilots on the performance of CAM. Therefore, we consider a simple receiver structure to obtain the upper performance bounds. In this way minimal implementation cost and extended battery life time are supported. Accordingly, we specify the following requirements and features in our system design:

- The CAM parameters, e.g. PFF and symbol duration, are chosen at the transmitter.
- The amount of redundant data transmission for interference mitigation should be kept to a minimum, thus we only tolerate only a maximum redundancy of one real symbol.
- Channel estimation is performed by the method of Least Squares (LS).
- ZF equalizer is used for the channel equalization.
- No iterative interference rejection schemes shall be applied at the receiver to keep mobile equipment hardware simple and low cost.

As FBMC-OQAM suffers from intrinsic interference, several interference mitigation schemes for scattered pilots have been proposed in literature [18]–[28], which can be categorized as follows:

- Auxiliary Pilot (AP)
- Data Spreading (DS)
- Pairs of Pilots (POP)
- Pilot Clustering (PC)
- Basic Iterative Interference Mitigation (BIIM)
- Composite Pilot Pairs (CPP).

Referring to the system requirements defined above, both latter schemes are based on iterative channel estimation, equalization and data symbol detection and thus are not within the scope of our investigation. The channel estimation schemes proposed in [20]–[24] require more than one redundant symbol or do not provide a closed form solution and thus go beyond the scope of this paper. The POP scheme and the modified version of it, proposed in [26] and [27], respectively, provide a closed form LS estimation for the equalizer, whereas the AP [18] and DS [19] approaches considered within the context of our contribution both deliver a LS estimate of the channel. In fact, even though the estimation technique is similar for all of these schemes, it should be made clear that two different LS problem formulations (cost functions) are being raised. In other words, the POP scheme additionally requires the inverse equalizer determination, which might result in further errors, e.g. noise enhancement. Therefore, as a first step, the focus of our contribution is guided by the evaluation of AP and DS interference mitigation performance in terms of the channel estimation error for various PFFs. Doing so we want to answer the research question, whether the usage of CAM can provide sufficient gains compared to current "one-fits-all" approach when we have imperfect channel knowledge at the receiver. Therefore, analytical descriptions for the estimation errors are derived and the system level performance in terms of BER is determined and compared.

The rest of this paper is organized as follows. In section II, the FBMC-OQAM system model and the related intrinsic interference are reviewed. This is followed by an overview of the lattice and pulse shape adaptation theory in section III. The analytical descriptions of the channel estimation error in doubly dispersive channels are derived in section IV and the influence of the channel estimation error on the system performance is discussed in section V. Finally, a conclusion is drawn and future work is outlined.

Notation: $\mathbf{E}[\bullet]$ is the expected value, $\Re\{\bullet\}$ and $\Im\{\bullet\}$ are the real and imaginary parts, respectively, $*$ denotes the convolution operation and $\delta_{a,b}$ is the Kronecker-Delta with respect to a and b. Variables in blackboard bold, e.g. $\mathbb{M}$, denote sets and $\times$ is used for the Cartesian product of sets. Underlined lower case letters, e.g. $\underline{d}$ are used to indicate vectors, underlined capitals, e.g. $\underline{C}$ are used for matrices. $(\bullet)^T$ and $(\bullet)^H$ are the transposition

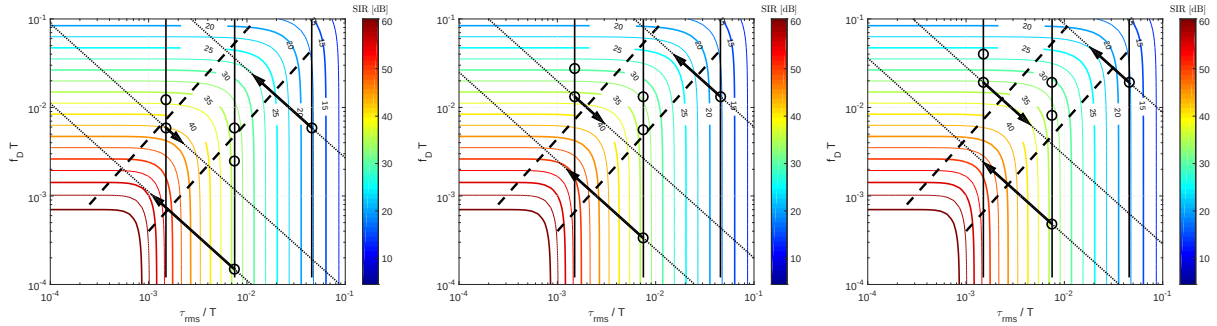

(a) 800 MHz (b) 1800 MHz (c) 2600 MHz

Fig. 1. Reconstruction performance (SIR [13]) as a function of the normalized delay spread τ_{rms}/T and maximum Doppler shift $f_D T$ of an FBMC-OQAM system with $K = 256$ subcarriers and symbol duration T, operating in channels with exponential PDP and Jakes Doppler PSD. The vertical lines indicate the SIR values for the channel environments defined in [29] (left: Rax, middle: Tux, right: HTx), which are achievable by an LTE system with standard conform T. The circles show the resulting operation points for the default mobile speeds [29] at the typical frequency bands for LTE in Europe. The area between the dashed diagonals indicates the optimal operation region in terms of SIR after the AFB of an FBMC-OQAM system utilizing the PHYDYAS pulse shape. The dotted diagonals depict the SIR values for a certain operation point, if the symbol duration T of the LTE system is adjusted to maximize the SIR. The arrows indicate the direction of available SIR gains for the present channel scenario.

and conjugate transposition, respectively. Continuous-time signals are presented by parenthesis and discrete-time signals with brackets by omitting the sample period T_s, e.g. $s[n] := s(nT_s)$. Algorithm specific solutions for a certain variable are determined by an exponential identifier in braces, e.g. $\varepsilon^{\{\bullet\}}$.

II. System Model

Here, a description of the applied system and channel models is provided. Subsequently, the expression for an FBMC-OQAM symbol distorted by a doubly dispersive channel is recalled. The receiver noise is neglected in our work, as only the effects of the intrinsic interference in FBMC-OQAM systems, as well as ISI and ICI caused by the propagation channel, are in the focus of interest. In our investigation, we consider a critically sampled discrete-time system model, i.e. $T_s = T/K$ and $t = nT_s$ with the sampling period T_s, symbol duration T and total number of subcarriers K as depicted in Figure 2.

A. Discrete-Time Model

Considering the time-variant multipath channel $h[\tau, n]$ of path delay τ, the received signal $r[n]$ can be expressed by

$$r[n] = h[\tau, n] * s[n], \tag{1a}$$

where the transmit signal $s[n]$ is given by

$$s[n] = \sum_{(m,k)\in\mathbb{T}} \theta_{m,k} a_{m,k} f_k[n - mM_0] \tag{1b}$$

$$\text{with} \quad f_k[n] = f[n] \mathrm{e}^{\mathrm{j}2\pi k K_0 n} \tag{1c}$$

$$\text{and} \quad \theta_{m,k} = \mathrm{j}^{m+k}. \tag{1d}$$

Here, $a_{m,k}$ is an independent and identically distributed (i.i.d.) real valued OQAM symbol transmitted at time index m out of a set of allocated symbols $\mathbb{M}$ and on the subcarrier index k out of a set of allocated subcarriers $\mathbb{K}$, which is modulated on the transmitter PFF $f_k[n]$. $\mathbb{T} = \mathbb{M} \times \mathbb{K}$ denotes the set of transmit position tuples (m, k). τ_0 and ν_0 are the normalized symbol and subcarrier spacing spanning the lattice grid, respectively. $K_0 = \nu_0/K = \nu_0 T_s/T$ and $M_0 = \tau_0 K = \tau_0 T/T_s$ define the effective subcarrier and symbol spacing used for the OQAM modulation. $\theta_{m,k}$ is a phase shift required to fulfill the real orthogonality condition.

The discrete-time channel modeled by a time-variant tapped delay line with a maximum Doppler shift f_D is given as follows:

$$h[\tau, n] = \sum_{l=0}^{L-1} h_l[n] \delta[\tau - \tau_l], \tag{2}$$

where $h_l[n]$ is a time-dependent complex valued channel coefficient with the delay τ_l at the channel tap index l out of L channel taps. The delay spread τ_{rms} of the channel is given by [30]

$$\tau_{\text{rms}} = \sqrt{\frac{\sum_{l=0}^{L-1} g_l \tau_l^2}{\sum_{l=0}^{L-1} g_l} - \bar{\tau}^2}, \tag{3}$$

where the mean delay $\bar{\tau}$ is given by [30]

$$\bar{\tau} = \frac{\sum_{l=0}^{L-1} g_l \tau_l}{\sum_{l=0}^{L-1} g_l}. \tag{4}$$

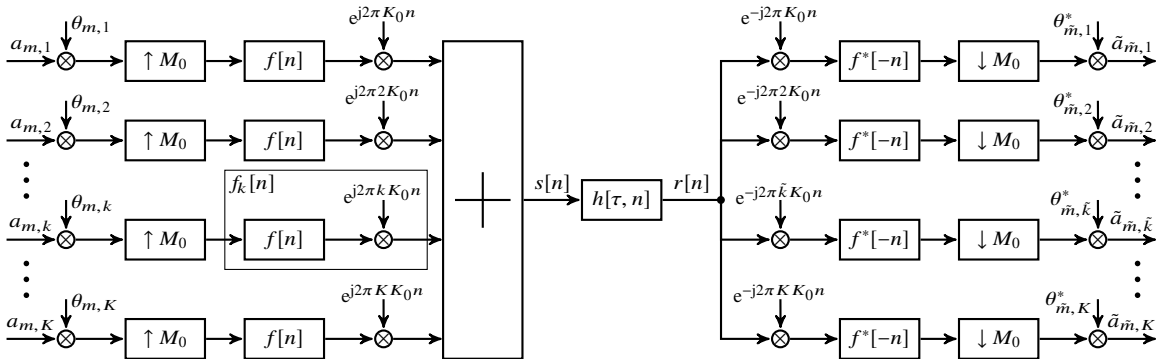

Fig. 2. Generic discrete-time transceiver chain for a multicarrier scheme with K subcarriers and a lattice grid defined by a symbol spacing of M_0 and subcarrier spacing K_0. The weighting factor $\theta_{m,k}$ is a phase shift used to establish the real orthogonality needed for symbols $a_{m,k} \in \mathbb{R}$.

$g_l = \mathbf{E}\left[|h_l[n]|^2\right]$ is the value of the l-th tap of the PDP. All results obtained in this contribution rely on the exponential decay PDP and the Jakes Doppler PSD $D(\nu)$ given by [30]

$$g_l = \frac{1}{K\tau_{\mathrm{rms}}/T}\mathrm{e}^{-\frac{\tau_l}{K\tau_{\mathrm{rms}}/T}} \tag{5a}$$

$$\text{and} \quad D(\nu) = \frac{1}{\pi f_D T\sqrt{1-\left(\frac{\nu}{f_D T}\right)^2}}. \tag{5b}$$

B. Received Symbol

To obtain the unequalized data or pilot symbol $\tilde{a}_{\tilde{m},\tilde{k}}$, a matched filter is applied to $r[n]$ and the phase shift $\theta_{m,k}$ is reversed. Accordingly, under assumption of perfect synchronization to the first channel tap, $\tilde{a}_{\tilde{m},\tilde{k}}$ can be written by

$$\begin{aligned}\tilde{a}_{\tilde{m},\tilde{k}} &= \theta^*_{\tilde{m},\tilde{k}}\left(r[n] * f^*_{\tilde{k}}[\tilde{m}M_0 - n]\right)\Big\downarrow_{M_0}\\ &= \theta^*_{\tilde{m},\tilde{k}}\Bigg(\sum_{(m,k)\in\mathbb{T}}\theta_{m,k}a_{m,k}\Big(h[\tau,n] * f_k[n-mM_0]\Big)\\ &\quad * f^*_{\tilde{k}}[\tilde{m}M_0 - n]\Bigg)\Big\downarrow_{M_0},\end{aligned} \tag{6}$$

with $\tilde{m}$ and $\tilde{k}$ being the symbol and subcarrier index of the demodulated received symbol, respectively. As long as $2f_D T_s < 1$, the Discrete-Time Fourier Transform (DTFT) can be applied to $h[\tau, n]$ [30]. Therefore, and by consideration of (2), (6) yields

$$\begin{aligned}\tilde{a}_{\tilde{m},\tilde{k}} &= \theta^*_{\tilde{m},\tilde{k}}\sum_{(m,k)\in\mathbb{T}}\theta_{m,k}a_{m,k}\Bigg(\Bigg(\sum_{l=0}^{L-1}h[\tau_l,n]\\ &\quad\cdot f_k[n-\tau_l-mM_0]\Bigg) * f^*_{\tilde{k}}[\tilde{m}M_0-n]\Bigg)\Big\downarrow_{M_0}\\ &= \theta^*_{\tilde{m},\tilde{k}}\sum_{(m,k)\in\mathbb{T}}\theta_{m,k}a_{m,k}\Bigg(\Bigg(\sum_{l=0}^{L-1}\int_{-f_D}^{f_D}h_D[\tau_l,\nu]\mathrm{e}^{\mathrm{j}2\pi n\nu}\\ &\quad\cdot f_k[n-\tau_l-mM_0]\,\mathrm{d}\nu\Bigg) * f^*_{\tilde{k}}[\tilde{m}M_0-n]\Bigg)\Big\downarrow_{M_0},\end{aligned} \tag{7}$$

with $h_D[\tau_l, \nu]$ being the Doppler-variant channel impulse response or spreading function given by

$$h_D[\tau_l,\nu] = \sum_{n=-\infty}^{\infty}h[\tau_l,n]\mathrm{e}^{-\mathrm{j}2\pi n\nu}. \tag{8}$$

We represent the symbol index offset by $\mu = m - \tilde{m}$, the subcarrier offset by $\kappa = k - \tilde{k}$ and the related sets of available offsets by $\tilde{\mathbb{M}} = \mathbb{M} - \tilde{m}$ and $\tilde{\mathbb{K}} = \mathbb{K} - \tilde{k}$. The $\tilde{a}_{\tilde{m},\tilde{k}}$ related lattice grid can be described by the set of lattice position tuples $(\mu, \kappa) \in \mathbb{S}$ with $\mathbb{S} = (\tilde{\mathbb{M}} \times \tilde{\mathbb{K}})$. Moreover, with definition of the set of neighboring symbols as $\mathbb{S}_N = \mathbb{S} \setminus (0,0)$, $\tilde{a}_{\tilde{m},\tilde{k}}$ yields

$$\begin{aligned}\tilde{a}_{\tilde{m},\tilde{k}} &= \sum_{(\mu,\kappa)\in\mathbb{S}}\theta_{\mu,\kappa}a_{\tilde{m}+\mu,\tilde{k}+\kappa}\\ &\quad\cdot\sum_{l=0}^{L-1}\int_{-f_D}^{f_D}h_D[\tau_l,\nu]\mathrm{e}^{\mathrm{j}2\pi\tilde{m}M_0\nu}A^{\tilde{k}}_{\mu,\kappa}[\tau_l,\nu]\,\mathrm{d}\nu\\ &= \underbrace{a_{\tilde{m},\tilde{k}}H_{\tilde{m},\tilde{k}}(0,0)}_{\tilde{a}^{\{d\}}_{\tilde{m},\tilde{k}}} + \underbrace{\sum_{(\mu,\kappa)\in\mathbb{S}_N}\theta_{\mu,\kappa}a_{\tilde{m}+\mu,\tilde{k}+\kappa}H_{\tilde{m},\tilde{k}}(\mu,\kappa)}_{\tilde{a}^{\{I\}}_{\tilde{m},\tilde{k}}}.\end{aligned} \tag{9}$$

Here, $\tilde{a}^{\{d\}}_{\tilde{m},\tilde{k}}$ is the desired unequalized signal and $\tilde{a}^{\{I\}}_{\tilde{m},\tilde{k}}$ includes the ISI and ICI, respectively. $H_{\tilde{m},\tilde{k}}(\mu,\kappa)$ is the system dependent channel coefficient given by

$$H_{\tilde{m},\tilde{k}}(\mu,\kappa) = \sum_{l=0}^{L-1}\int_{-f_D}^{f_D}h_D[\tau_l,\nu]\mathrm{e}^{\mathrm{j}2\pi\tilde{m}M_0\nu}A^{\tilde{k}}_{\mu,\kappa}[\tau_l,\nu]\,\mathrm{d}\nu, \tag{10}$$

where the phase shifted discrete-time ambiguity function $A^{\tilde{k}}_{\mu,\kappa}[\tau_l, \nu]$ is defined by

$$\begin{aligned} A^{\tilde{k}}_{\mu,\kappa}[\tau_l, \nu] &= \sum_{n=-\infty}^{\infty} f[n-\mu M_0-\tau_l] f^*[n] \\ &\quad \cdot \mathrm{e}^{\mathrm{j}2\pi(K_0\kappa+\nu)n} \mathrm{e}^{-\mathrm{j}2\pi K_0(\tilde{k}+\kappa)(\mu M_0+\tau_l)} \\ &= A[\mu M_0+\tau_l, \kappa K_0+\nu] \mathrm{e}^{-\mathrm{j}2\pi K_0(\tilde{k}+\kappa)(\mu M_0+\tau_l)}, \end{aligned} \tag{11}$$

with the discrete-time ambiguity function

$$A[\tau, \nu] = \sum_{n=-\infty}^{\infty} f[n-\tau] f^*[n] \mathrm{e}^{\mathrm{j}2\pi\nu n}. \tag{12}$$

III. Lattice Grid and Pulse Shaping

To achieve a robust transmission over doubly dispersive channels, previous studies have shown that the direction parameter $\beta \in [0, \infty)$ of a PFF used for pulse shaping as well as the selection of the lattice grid defined by T_0 and F_0 should match the statistical properties of the channel environment [3], [34] as follows:

$$\frac{T_0}{F_0} \propto \frac{\tau_{\mathrm{rms}}}{f_D} \tag{13a}$$

$$\beta \propto \frac{\tau_{\mathrm{rms}}}{f_D}. \tag{13b}$$

The direction parameter β is defined by

$$\beta = \frac{\sigma_t}{\sigma_f}, \tag{14}$$

where σ_t and σ_f are the standard deviation (or dispersion) of the applied PFF in time- and frequency domain, respectively. Both relations in (13) have to be fulfilled jointly, as β and T_0, i.e. PFF and symbol duration, are selected conjoint during a system design.

A. Lattice Grid

The most obvious way of adapting a system to a certain channel environment is to match the symbol duration and subcarrier spacing accordingly (CASS). Considering practical constraints such as implementation complexity, oscillator accuracy and processing clock speed, it is not reasonable to design communication systems with the capability of arbitrary adjustment of the symbol duration. The usage of exponential subcarrier spacing granularities based on a power of two as proposed in [17] is seen as an evident approach. This can be implemented simply by means of a Fast Fourier Transform (FFT) with maximum required length. However, this is a suboptimal method, since (13a) cannot be fulfilled by a system designed to operate in various channel environments. A more accurate system adaptation can be provided by the application of a suitable PFF as given by (13b) (CASS + CAPS $\rightarrow$ CAM).

B. Pulse Shaping

In system design, the selection of a PFF is restricted by the overlapping factor, γ, which specifies the amount of overlapping symbols and the occupied bandwidth. These parameters directly affect the system latency as well as the out-of-band emissions and thus guard band sizes. The PFFs $f[n]$ applied in this work are derived from time-unlimited base PFFs $p[n]$ proposed in literature for FBMC-OQAM systems as follows:

$$f[n] = \begin{cases} p[n], & \frac{\gamma K}{2} \leq n < \frac{\gamma K}{2} \\ 0, & \text{otherwise} \end{cases}. \tag{15}$$

As base PFFs $p[n]$, we consider the Nyquist pulses, namely PHYDYAS [31] or Mirabbasi-Martin [35], an IOTA PFF based on EGF [32] and the Hermite pulse shape [33], which are summarized in Table I.

IV. Channel Estimation

In a multicarrier system the channel estimation is usually carried out in the frequency domain and is based on a transmitted reference sequence, which is either a separate preamble sequence or a number of scattered pilots within the whole transmission frame as done in LTE or DVB-T. Using the LS estimator, the channel coefficients $\tilde{H}_{\tilde{m},\tilde{k}}$ are calculated by comparing the received pilot symbol, i.e. $\tilde{a}_{\tilde{m},\tilde{k}} = \tilde{p}_{\tilde{m},\tilde{k}}$ and the reference symbol $p_{\tilde{m},\tilde{k}}$ according to

$$\tilde{H}_{\tilde{m},\tilde{k}} = \frac{\tilde{p}_{\tilde{m},\tilde{k}}}{p_{\tilde{m},\tilde{k}}}. \tag{16}$$

The resulting channel estimation error can be determined using the Mean-Squared Error (MSE) ε_H defined by

$$\varepsilon_H = \mathbf{E}\left[\left|\tilde{H}_{\tilde{m},\tilde{k}} - H_{\tilde{m},\tilde{k}}\right|^2\right]. \tag{17}$$

As shown in (9), each received data or pilot symbol can be considered as a superposition of a desired part and an interference part, which degrades the channel estimation accuracy. To enable a precise channel estimation, the transmission of each pilot symbol requires special processing to mitigate the interference. Various schemes have been proposed in literature to minimize the interference in preambles [36]–[40]. However, some systems such as LTE and DVB-T don't have a dedicated preamble. Additionally, almost every wireless communication system requires reference symbols embedded within the data part for the purpose of residual Carrier Frequency Offset (CFO) estimation and channel tracking.
Similar to (9), the estimated channel coefficient $\tilde{H}_{\tilde{m},\tilde{k}}$ can be considered as a linear combination as follows:

$$\tilde{H}_{\tilde{m},\tilde{k}} = H_{\tilde{m},\tilde{k}} + C_{\tilde{m},\tilde{k}} + R_{\tilde{m},\tilde{k}}, \tag{18}$$

so that (17) can be rewritten by

$$\varepsilon_H^{\{\mathrm{AP}\}} = \mathbf{E}\left[\left|C_{\tilde{m},\tilde{k}} + R_{\tilde{m},\tilde{k}}\right|^2\right]. \tag{19}$$

TABLE I
OVERVIEW OF THE APPLIED PROTOTYPE FILTERS INCLUDING THE DIRECTION PARAMETER β.

Filter	Analytical description	Parameters	β ($\gamma = 4$)
PHYDYAS [31]	$p[n] = q_0 + 2\sum_{i=1}^{\gamma-1} q_i \cos\left[\frac{2\pi i n}{\gamma K}\right]$	γ	1.6729
EGF [32]	$p[n,\alpha] = \frac{1}{2}\sum_{i=0}^{\infty} q_{i,\alpha,\nu_0}\left[g_\alpha\left[\frac{n}{K}+\frac{i}{\nu_0}\right]+g_\alpha\left[\frac{n}{K}-\frac{i}{\nu_0}\right]\right] \cdot \sum_{i'=0}^{\infty} q_{i',1/\alpha,\tau_0}\cos\left[\frac{2\pi i' n}{M_0}\right]$ with $g_\alpha[n] = (2\alpha)^{\frac{1}{4}} \mathrm{e}^{-\pi\alpha\left(\frac{n}{K}\right)^2}$	α	$\alpha = 1 : 1.7201$ $\alpha = 2 : 0.99995$ $\alpha = 3 : 0.70906$
Hermite [33]	$p[n] = \sum_{i=0}^{N_H-1} a_{4i} H_{4i}\left[2\sqrt{\pi}\frac{n}{K}\right]$ with $H_i[n] = \mathrm{e}^{-\frac{n^2}{2}}\left[\frac{\mathrm{d}^i}{\mathrm{d}t^i}\mathrm{e}^{-t^2}\right]_{t=nT_s}$	N_H	1

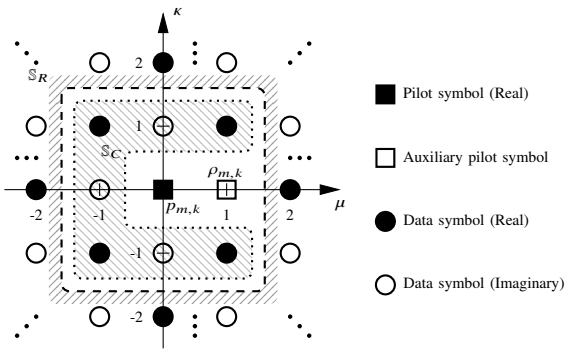

Fig. 3. Allocation pattern of pilot symbol $p_{m,k}$ and AP $\rho_{m,k}$ for $(\mu_a, \kappa_a) = (1, 0)$. Data symbols within the inner hatched area are used for the AP calculation as reported in [18].

$C_{\tilde{m},\tilde{k}}$ represents the residual interference induced by the symbols considered by an interference mitigation scheme to combat the interference on $\tilde{p}_{\tilde{m},\tilde{k}}$. $R_{\tilde{m},\tilde{k}}$ is the interference imposed by all symbols not included in the interference mitigation.

A. Auxiliary Pilot (AP)

To reduce the interference on pilot symbols, Javaudin et al. [18] proposed the usage of a help pilot $\rho_{m,k}$. The more common naming AP has been introduced in [39]. The AP is placed at the lattice position with symbol offset μ_a and subcarrier offset κ_a relative to the associated pilot symbol position, as depicted in Figure 3. Assuming that $\tau_{\mathrm{rms}} \ll T$ and $f_D \ll 1/T$, with $\mathbb{S}_C \subseteq \{\mathbb{S}_N \backslash (\mu_a, \kappa_a)\}$ being the set of symbols considered for interference mitigation, the AP approach is specified by

$$\sum_{(\mu,\kappa)\in\mathbb{S}_C} \theta_{\mu,\kappa} a_{m+\mu,k+\kappa} A^k_{\mu,\kappa}[0,0] + \rho_{m,k} A^k_{\mu_a,\kappa_a}[0,0] = 0. \quad (20)$$

Therefore, for pilot symbol $p_{m,k}$, $\rho_{m,k}$ yields

$$\rho_{m,k} = -\sum_{(\mu,\kappa)\in\mathbb{S}_C} \theta_{\mu,\kappa} a_{m+\mu,k+\kappa} \frac{A^k_{\mu,\kappa}[0,0]}{A^k_{\mu_a,\kappa_a}[0,0]}, \quad (21)$$

where the average power $P^{\{\mathrm{AP}\}}$ of $\rho_{m,k}$ is

$$P^{\{\mathrm{AP}\}} = \mathbf{E}\left[\rho_{m,k}\rho^*_{m,k}\right] = \sigma_d^2 \sum_{(\mu,\kappa)\in\mathbb{S}_C} \frac{|A_{\mu,\kappa}[0,0]|^2}{|A_{\mu_a,\kappa_a}[0,0]|^2}, \quad (22)$$

with the average data symbol power $\sigma_d^2 = \mathbf{E}\left[|a_{m,k}|^2\right]$. Applying this generalized approach for APs, each part of (18) can be defined by

$$H_{\tilde{m},\tilde{k}} = H_{\tilde{m},\tilde{k}}(0,0) \quad (23a)$$

$$C_{\tilde{m},\tilde{k}} = \frac{\rho_{\tilde{m},\tilde{k}}}{p_{\tilde{m},\tilde{k}}} H_{\tilde{m},\tilde{k}}(\mu_a,\kappa_a) + \sum_{(\mu,\kappa)\in\mathbb{S}_C} \theta_{\mu,\kappa} \frac{a_{\tilde{m}+\mu,\tilde{k}+\kappa}}{p_{\tilde{m},\tilde{k}}} H_{\tilde{m},\tilde{k}}(\mu,\kappa) \quad (23b)$$

$$R_{\tilde{m},\tilde{k}} = \sum_{(\mu,\kappa)\in\mathbb{S}_R} \theta_{\mu,\kappa} \frac{a_{\tilde{m}+\mu,\tilde{k}+\kappa}}{p_{\tilde{m},\tilde{k}}} H_{\tilde{m},\tilde{k}}(\mu,\kappa), \quad (23c)$$

where $\mathbb{S}_R = \mathbb{S}_N \setminus \{\mathbb{S}_C, (\mu_a,\kappa_a)\}$. According to (19), the channel estimation error for the AP scheme $\varepsilon_H^{\{\mathrm{AP}\}}$ is

calculated by

$$\varepsilon_H^{\{\mathrm{AP}\}} = \mathbf{E}\Bigg[\Bigg| \sum_{(\mu,\kappa)\in\mathbb{S}_R} \theta_{\mu,\kappa} \frac{a_{\tilde{m}+\mu,\tilde{k}+\kappa}}{p_{\tilde{m},\tilde{k}}} H_{\tilde{m},\tilde{k}}(\mu,\kappa) + \sum_{(\mu,\kappa)\in\mathbb{S}_C} \theta_{\mu,\kappa} \frac{a_{\tilde{m}+\mu,\tilde{k}+\kappa}}{p_{\tilde{m},\tilde{k}}} \hat{H}_{\tilde{m},\tilde{k}}(\mu,\kappa)\Bigg|^2\Bigg], \quad (24)$$

with

$$\hat{H}_{\tilde{m},\tilde{k}}(\mu,\kappa) = H_{\tilde{m},\tilde{k}}(\mu,\kappa) - \frac{A_{\mu,\kappa}^{\tilde{k}+\kappa}[0,0]}{A_{\mu_a,\kappa_a}^{\tilde{k}+\kappa_a}[0,0]} H_{\tilde{m},\tilde{k}}(\mu_a,\kappa_a). \quad (25)$$

In [18] only OQAM symbols next to the pilot symbol are considered for the calculation of $\rho_{m,k}$, i.e. $\mathbb{S}_C = (\{-1,0,1\}\times\{-1,0,1\}) \setminus \{(0,0),(\mu_a = 1,\kappa_a = 0)\}$. Referring to the derivations in appendix A and B, $\varepsilon_H^{\{\mathrm{AP}\}}$ yields

$$\varepsilon_H^{\{\mathrm{AP}\}} = \frac{1}{b}\sum_{l=0}^{L-1}\int_{-f_D}^{f_D} g_l D(\nu)\alpha[\tau_l,\nu]\,\mathrm{d}\nu \quad (26)$$

$$= \varepsilon_c^{\{\mathrm{AP}\}} + \varepsilon_r^{\{\mathrm{AP}\}}, \quad (27)$$

with the pilot boost factor $b = \sigma_p^2/\sigma_d^2$ and the average pilot symbol power $\sigma_p^2 = \mathbf{E}\left[|p_{m,k}|^2\right]$. The cancellation error $\varepsilon_c^{\{\mathrm{AP}\}}$ is given by

$$\varepsilon_c^{\{\mathrm{AP}\}} = \frac{1}{b}\sum_{l=0}^{L-1}\int_{-f_D}^{f_D} g_l D(\nu) \sum_{(\mu,\kappa)\in\mathbb{S}_C} \left|\alpha_{\mu,\kappa}[\tau_l,\nu]\right|^2 \mathrm{d}\nu \quad (28)$$

and the residual estimation error $\varepsilon_r^{\{\mathrm{AP}\}}$ induced by symbols not considered by the interference mitigation scheme is obtained by:

$$\varepsilon_r^{\{\mathrm{AP}\}} = \frac{1}{b}\sum_{l=0}^{L-1}\int_{-f_D}^{f_D} g_l D(\nu) \sum_{(\mu,\kappa)\in\mathbb{S}_R} \left|A_{\mu,\kappa}[\tau_l,\nu]\right|^2 \mathrm{d}\nu. \quad (29)$$

The effective ambiguity functions $\alpha_{\mu,\kappa}[\tau_l,\nu]$ and $\alpha[\tau_l,\nu]$ are defined according to

$$\alpha_{\mu,\kappa}[\tau_l,\nu] = A_{\mu,\kappa}[\tau_l,\nu] - \frac{A_{\mu,\kappa}[0,0]}{A_{\mu_a,\kappa_a}[0,0]} A_{\mu_a,\kappa_a}[\tau_l,\nu] \quad (30)$$

and

$$\alpha[\tau_l,\nu] = \sum_{(\mu,\kappa)\in\mathbb{S}_C} \left|\alpha_{\mu,\kappa}[\tau_l,\nu]\right|^2 + \sum_{(\mu,\kappa)\in\mathbb{S}_R} \left|A_{\mu,\kappa}[\tau_l,\nu]\right|^2. \quad (31)$$

In (30) and (31) the discrete-time ambiguity function can be applied, as the delay and subcarrier specific phase shifts are either canceled out or removed due to the calculation of the absolute value.

The total channel estimation error $\varepsilon_H^{\{\mathrm{AP}\}}$ of the AP scheme and both parts $\varepsilon_c^{\{\mathrm{AP}\}}$ and $\varepsilon_r^{\{\mathrm{AP}\}}$ are depicted in Figure 4 for different PFFs. Considering $\varepsilon_c^{\{\mathrm{AP}\}}$ in Figure 4a, 4d, 4g and 4j, the AP scheme can provide almost a perfect interference mitigation. As the utilized channel is not considered by the AP scheme, the channel estimation error increases similarly to the SIR of received data symbols shown in Figure 1. However, the overall channel estimation error $\varepsilon_H^{\{\mathrm{AP}\}}$ is severely limited, as the estimation error is bounded by $\varepsilon_r^{\{\mathrm{AP}\}}$ (see Figure 4b, 4e, 4h and 4k). For isotropic PFFs (i.e. EGF with $\alpha = 2$ and Hermite), the AP scheme delivers a minimum $\varepsilon_H^{\{\mathrm{AP}\}}$ of approximately -18 dB. For non-isotropic PFFs, $R_{\tilde{m},\tilde{k}}$ causes an increase of the channel estimation error to -11 dB and -14 dB for the PHYDYAS and EGF $\alpha = 3$ PFFs, respectively. Additionally, the transmit power is increased, as compared to classical CP-OFDM the pilot pair ($p_{m,k}$ and $\rho_{m,k}$) power is in average about 3-9 dB higher which may become an issue for high pilot pattern densities, as the effective data symbol Signal-to-Interference-plus-Noise Ratio (SINR) is decreased. For all PFFs, the channel estimation performance is limited by the residual estimation error $\varepsilon_r^{\{\mathrm{AP}\}}$ in the region of $\tau_{\mathrm{rms}}/T \leq 9\cdot10^{-3}$ and $f_D T \leq 3\cdot10^{-2}$. However, at the cost of increased system complexity and potentially latency, the channel estimation performance can be improved significantly if $R_{\tilde{m},\tilde{k}}$ is minimized by consideration of more symbols in interference mitigation as suggested in [41].

B. Data Spreading (DS)

Instead of using only one symbol to combat the interference on the pilot symbol as done in AP, Lélé et al. proposed in [19] to impose the zero forcing condition on a certain number of neighboring symbols $\Lambda > 1$, with $\mathbb{S}_C \subseteq \mathbb{S}_N$. This concept has been extended by [23], [24] to avoid the use of the auxiliary pilot and to improve the algorithms for the coding matrices design. In this work, we focus on the performance of the algorithm proposed in [19]. To simplify the notation, spread data symbols are indexed as depicted in Figure 5, with $\lambda : \{1,\ldots,\Lambda\} \rightarrow \{(\mu,\kappa)_\lambda\}$. Accordingly, the interference can be mitigated by

$$\sum_{(\mu,\kappa)\in\mathbb{S}_C} \theta_{\mu,\kappa} a_{m+\mu,k+\kappa} A_{\mu,\kappa}^k[0,0] = \sum_{\lambda=1}^{\Lambda} \theta_\lambda a_\lambda A_\lambda^k[0,0] = 0, \quad (32)$$

where a_λ are the spread data symbols calculated by

$$\underline{a} = \underline{C}\,\underline{d}, \quad (33)$$

with

$$a_\lambda = \underline{\chi}_\lambda\,\underline{d}. \quad (34)$$

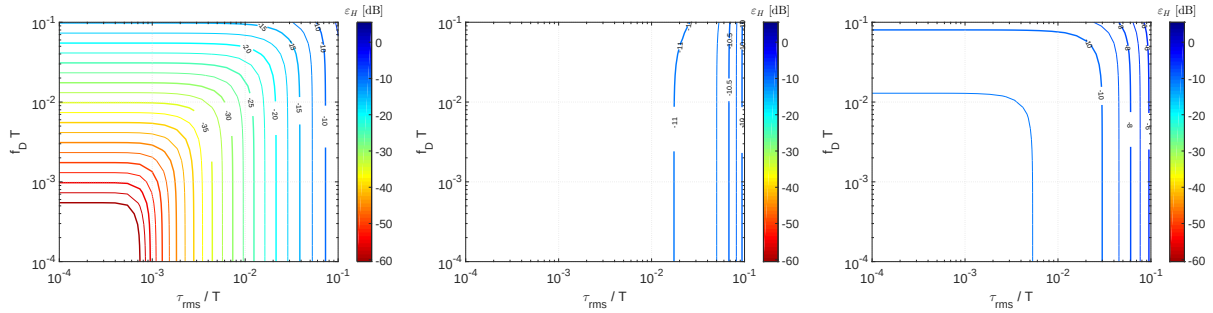

(a) $\boldsymbol{\varepsilon_c^{\{AP\}}}$ with PHYDYAS (b) $\boldsymbol{\varepsilon_r^{\{AP\}}}$ with PHYDYAS (c) $\boldsymbol{\varepsilon_H^{\{AP\}}}$ with PHYDYAS (2.76 dB)

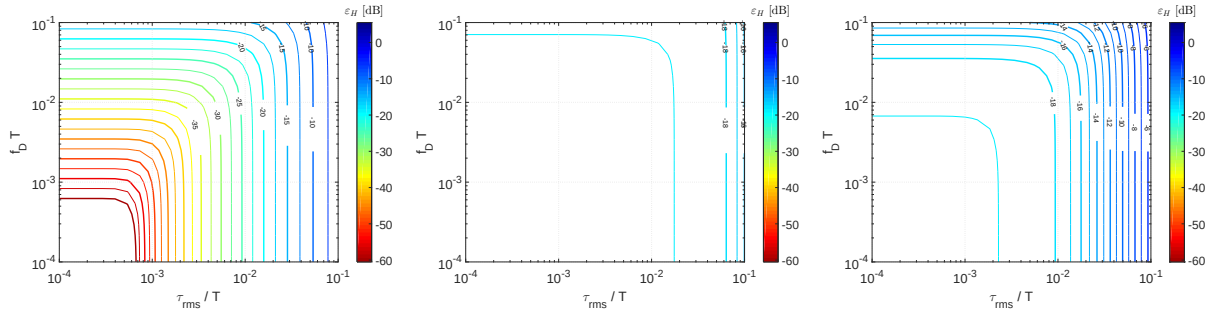

(d) $\boldsymbol{\varepsilon_c^{\{AP\}}}$ with Hermite (e) $\boldsymbol{\varepsilon_r^{\{AP\}}}$ with Hermite (f) $\boldsymbol{\varepsilon_H^{\{AP\}}}$ with Hermite (6.19 dB)

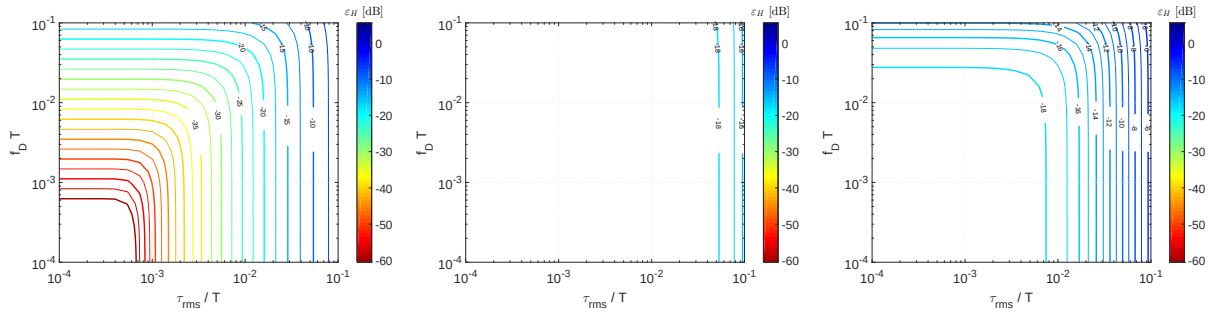

(g) $\boldsymbol{\varepsilon_c^{\{AP\}}}$ with EGF $\boldsymbol{\alpha} = 2$ (h) $\boldsymbol{\varepsilon_r^{\{AP\}}}$ with EGF $\boldsymbol{\alpha} = 2$ (i) $\boldsymbol{\varepsilon_H^{\{AP\}}}$ with EGF $\boldsymbol{\alpha} = 2$ (6.09 dB)

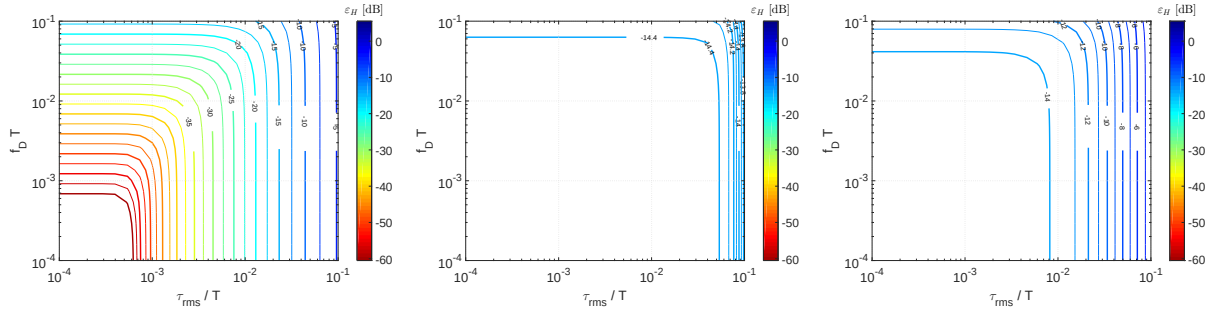

(j) $\boldsymbol{\varepsilon_c^{\{AP\}}}$ with EGF $\boldsymbol{\alpha} = 3$ (k) $\boldsymbol{\varepsilon_r^{\{AP\}}}$ with EGF $\boldsymbol{\alpha} = 3$ (l) $\boldsymbol{\varepsilon_H^{\{AP\}}}$ with EGF $\boldsymbol{\alpha} = 3$ (9.11 dB)

Fig. 4. Scattered pilot based channel estimation error of FBMC-OQAM systems for AP interference mitigation operating in various channel environments with $K = 256$, $\gamma = 4$ and $b = 1$. The cancellation error $\boldsymbol{\varepsilon_c^{\{AP\}}}$, the residual estimation error $\boldsymbol{\varepsilon_r^{\{AP\}}}$ and the total estimation error $\boldsymbol{\varepsilon_H^{\{AP\}}}$ are depicted in the left, middle and right column, respectively. The values in parentheses determine the required AP power increase per pilot symbol compared to the data symbols $a_{m,k}$.

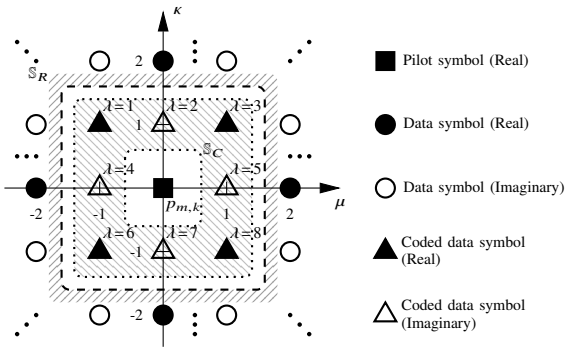

Fig. 5. Allocation and index pattern of pilot and data symbols for the DS scheme. All data symbols within the inner hatched area (i.e. $\Lambda = 8$) are spread to reduce the interference induced onto the pilot symbol $p_{m,k}$ [19].

Here, $\underline{d}$ is a vector of the original OQAM symbols and $\underline{C}$ is the spreading matrix including different spreading codes $\underline{c}_\lambda$ defined by

$$\underline{C} := [\underline{c}_1, \ldots, \underline{c}_\lambda, \ldots, \underline{c}_\Lambda] \tag{35a}$$

$$\underline{c}_\lambda := [c_{1,\lambda}, \ldots, c_{\lambda',\lambda}, \ldots, c_{\Lambda,\lambda}]^T \tag{35b}$$

$$\underline{\chi}_\lambda := [c_{\lambda,1}, \ldots, c_{\lambda,\lambda'}, \ldots, c_{\lambda,\Lambda}] \tag{35c}$$

$$\underline{d} := [d_1, \ldots, d_\lambda, \ldots, d_\Lambda]^T \tag{35d}$$

$$\underline{a} := [a_1, \ldots, a_\lambda, \ldots, a_\Lambda]^T \tag{35e}$$

To ensure that d_λ can be recovered on the receiver side as well as to avoid transmission power waste and noise enhancement, $\underline{C}$ has to be orthonormal [19]. Similar to the AP scheme, the DS approach requires a specific symbol d_Λ such that (32) is fulfilled for all d_λ. Here, d_Λ is a linear combination of all data symbols d_λ, i.e.

$$d_\Lambda = \sum_{\lambda=1}^{\Lambda-1} \beta_\lambda d_\lambda, \quad \beta_\lambda \in \mathbb{R}, \tag{36}$$

where β_λ is a weighting factor, which is an element of the weighting vector $\underline{\beta}$:

$$\underline{\beta} = [\beta_1, \ldots, \beta_{\Lambda-1}]. \tag{37}$$

With regard to this, the average power $P^{\{\mathrm{DS}\}}$ of d_Λ is given by

$$P^{\{\mathrm{DS}\}} = \mathbf{E}\left[d_\Lambda d_\Lambda^*\right] = \sigma_d^2 \underline{\beta}\,\underline{\beta}^T = \sigma_d^2 \sigma_\beta^2. \tag{38}$$

Considering the set $\mathbb{S}_C$, the different parts of (18) for the DS scheme are obtained as below:

$$H_{\tilde{m},\tilde{k}} = H_{\tilde{m},\tilde{k}}(0,0) \tag{39a}$$

$$\begin{aligned} C_{\tilde{m},\tilde{k}} &= \sum_{(\mu,\kappa)\in\mathbb{S}_C} \theta_{\mu,\kappa} \frac{a_{\tilde{m}+\mu,\tilde{k}+\kappa}}{p_{\tilde{m},\tilde{k}}} H_{\tilde{m},\tilde{k}}(\mu,\kappa) \\ &= \sum_{\lambda=1}^{\Lambda} H_\lambda \frac{a_\lambda}{p_{\tilde{m},\tilde{k}}} = \sum_{\lambda=1}^{\Lambda} H_\lambda \frac{\underline{\chi}_\lambda \underline{d}}{p_{\tilde{m},\tilde{k}}} \end{aligned} \tag{39b}$$

$$R_{\tilde{m},\tilde{k}} = \sum_{(\mu,\kappa)\in\mathbb{S}_R} \theta_{\mu,\kappa} \frac{a_{\tilde{m}+\mu,\tilde{k}+\kappa}}{p_{\tilde{m},\tilde{k}}} H_{\tilde{m},\tilde{k}}(\mu,\kappa), \tag{39c}$$

with $H_\lambda := \theta_{(\mu,\kappa)_\lambda} H_{\tilde{m},\tilde{k}}(\mu,\kappa)_\lambda$. According to (19), $\varepsilon_H^{\{\mathrm{DS}\}}$ is specified as

$$\begin{aligned} \varepsilon_H^{\{\mathrm{DS}\}} = \mathbf{E}\Bigg[\Bigg| &\sum_{(\mu,\kappa)\in\mathbb{S}_R} \theta_{\mu,\kappa} \frac{a_{\tilde{m}+\mu,\tilde{k}+\kappa}}{p_{\tilde{m},\tilde{k}}} H_{\tilde{m},\tilde{k}}(\mu,\kappa) \\ &+ \sum_{\lambda=1}^{\Lambda} H_\lambda \frac{\underline{\chi}_\lambda \underline{d}}{p_{\tilde{m},\tilde{k}}}\Bigg|^2\Bigg]. \end{aligned} \tag{40}$$

Utilizing the derivations in appendix B and C, $\varepsilon_H^{\{\mathrm{DS}\}}$ yields

$$\begin{aligned} \varepsilon_H^{\{\mathrm{DS}\}} &= \frac{1}{b} \sum_{l=0}^{L-1} \int_{-f_D}^{f_D} g_l D(\nu) \\ &\quad \cdot \left(\sum_{(\mu,\kappa)\in\{\mathbb{S}_C,\mathbb{S}_R\}} |A_{\mu,\kappa}[\tau_l,\nu]|^2 + \underline{\alpha}_{\tau_l,\nu} \underline{X}\, \underline{\alpha}_{\tau_l,\nu}^H \right) \mathrm{d}\nu \end{aligned} \tag{41}$$

$$= \varepsilon_c^{\{\mathrm{DS}\}} + \varepsilon_r^{\{\mathrm{DS}\}}. \tag{42}$$

Here, the cancellation error $\varepsilon_c^{\{\mathrm{DS}\}}$ and the residual estimation error $\varepsilon_r^{\{\mathrm{DS}\}}$ are given by

$$\begin{aligned} \varepsilon_c^{\{\mathrm{DS}\}} = &\frac{1}{b} \sum_{l=0}^{L-1} \int_{-f_D}^{f_D} g_l D(\nu) \Bigg(\sum_{(\mu,\kappa)\in\mathbb{S}_C} |A_{\mu,\kappa}[\tau_l,\nu]|^2 \\ &+ \underline{\alpha}_{\tau_l,\nu} \underline{X}\, \underline{\alpha}_{\tau_l,\nu}^H \Bigg) \mathrm{d}\nu \end{aligned} \tag{43}$$

and

$$\varepsilon_r^{\{\mathrm{DS}\}} = \frac{1}{b} \sum_{l=0}^{L-1} \int_{-f_D}^{f_D} g_l D(\nu) \sum_{(\mu,\kappa)\in\mathbb{S}_R} \left|A_{\mu,\kappa}[\tau_l,\nu]\right|^2 \mathrm{d}\nu = \varepsilon_c^{\{\mathrm{AP}\}}. \tag{44}$$

In appendix C, $\underline{\alpha}_{\tau_l,\nu}$, $\underline{B}_I$ and $\underline{X}$ are given by (63) and (66). Like the AP scheme, [19] proposed only the usage of OQAM symbols next to the pilot symbol, i.e. $\Lambda = 8$ and $\mathbb{S}_C = (\{-1,0,1\} \times \{-1,0,1\}) \setminus (0,0)$, so that $\varepsilon_r^{\{\mathrm{DS}\}} = \varepsilon_r^{\{\mathrm{AP}\}}$. The appropriate spreading codes and the derived matrix $\underline{X}$ are provided in appendix D. The resulting cancellation and total channel estimation errors $\varepsilon_c^{\{\mathrm{DS}\}}$ and $\varepsilon_H^{\{\mathrm{DS}\}}$ are depicted in Figure 6, which additionally presents the performance ratio between the DS and AP schemes defined as below:

$$\Delta\varepsilon_H = \frac{\varepsilon_H^{\{\mathrm{DS}\}}}{\varepsilon_H^{\{\mathrm{AP}\}}} \text{ and } \Delta\varepsilon_c = \frac{\varepsilon_c^{\{\mathrm{DS}\}}}{\varepsilon_c^{\{\mathrm{AP}\}}}. \tag{45}$$

Because of $\varepsilon_r^{\{\mathrm{DS}\}} = \varepsilon_r^{\{\mathrm{AP}\}}$, the graphical presentation of $\varepsilon_r^{\{\mathrm{DS}\}}$ is omitted. Since the utilized channel is not considered in the design of the auxiliary data symbol

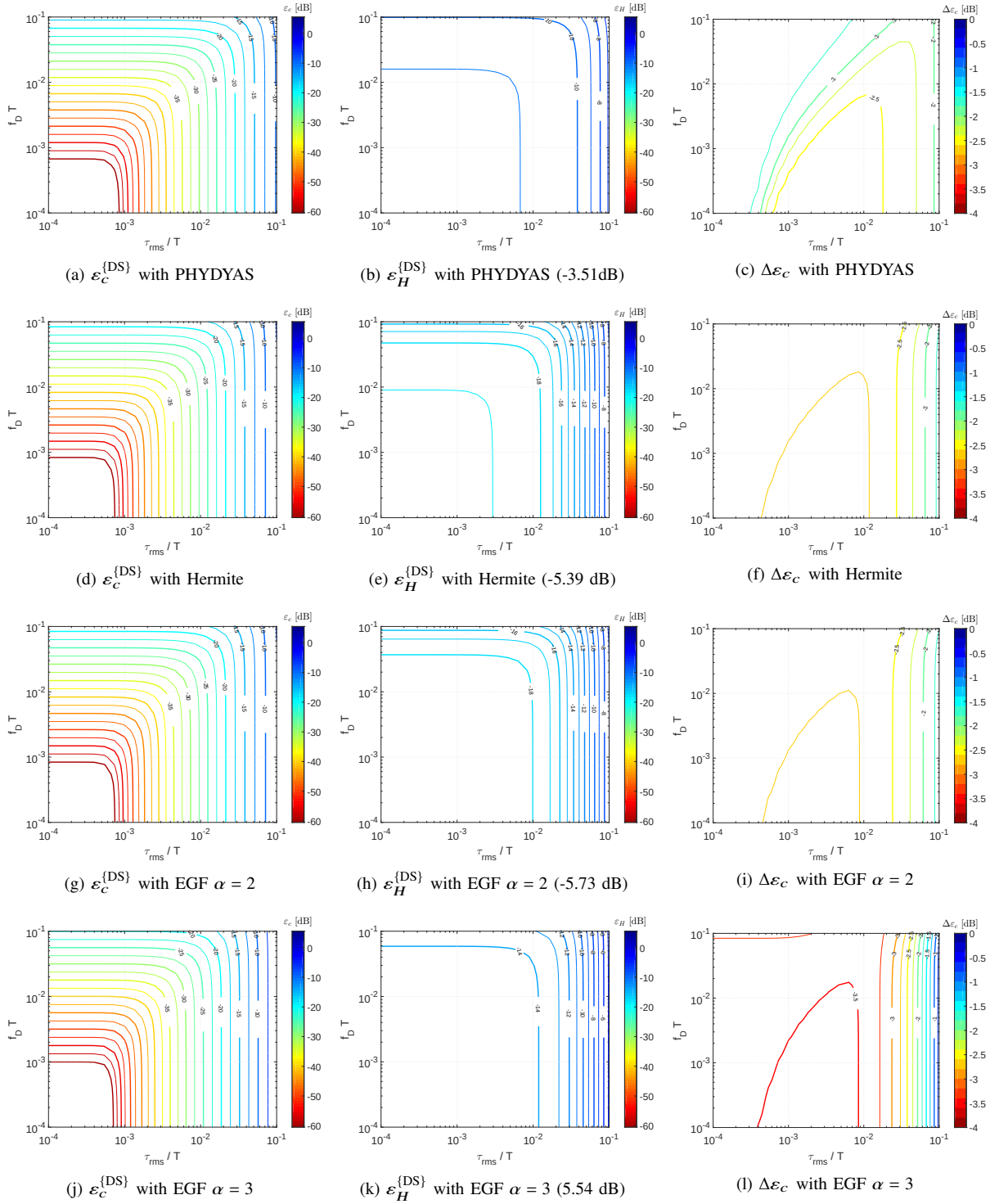

(a) $\boldsymbol{\varepsilon}_{\boldsymbol{c}}^{\{\mathrm{DS}\}}$ with PHYDYAS (b) $\boldsymbol{\varepsilon}_{\boldsymbol{H}}^{\{\mathrm{DS}\}}$ with PHYDYAS (-3.51dB) (c) $\Delta\boldsymbol{\varepsilon}_{\boldsymbol{c}}$ with PHYDYAS

(d) $\boldsymbol{\varepsilon}_{\boldsymbol{c}}^{\{\mathrm{DS}\}}$ with Hermite (e) $\boldsymbol{\varepsilon}_{\boldsymbol{H}}^{\{\mathrm{DS}\}}$ with Hermite (-5.39 dB) (f) $\Delta\boldsymbol{\varepsilon}_{\boldsymbol{c}}$ with Hermite

(g) $\boldsymbol{\varepsilon}_{\boldsymbol{c}}^{\{\mathrm{DS}\}}$ with EGF $\boldsymbol{\alpha} = 2$ (h) $\boldsymbol{\varepsilon}_{\boldsymbol{H}}^{\{\mathrm{DS}\}}$ with EGF $\boldsymbol{\alpha} = 2$ (-5.73 dB) (i) $\Delta\boldsymbol{\varepsilon}_{\boldsymbol{c}}$ with EGF $\boldsymbol{\alpha} = 2$

(j) $\boldsymbol{\varepsilon}_{\boldsymbol{c}}^{\{\mathrm{DS}\}}$ with EGF $\boldsymbol{\alpha} = 3$ (k) $\boldsymbol{\varepsilon}_{\boldsymbol{H}}^{\{\mathrm{DS}\}}$ with EGF $\boldsymbol{\alpha} = 3$ (5.54 dB) (l) $\Delta\boldsymbol{\varepsilon}_{\boldsymbol{c}}$ with EGF $\boldsymbol{\alpha} = 3$

Fig. 6. Scattered pilot based channel estimation error of FBMC-OQAM systems with DS interference mitigation operating in various channel environments with $K = 256$, $\gamma = 4$ and $b = 1$. The cancellation error $\boldsymbol{\varepsilon}_{\boldsymbol{c}}^{\{\mathrm{DS}\}}$, the total estimation error $\boldsymbol{\varepsilon}_{\boldsymbol{H}}^{\{\mathrm{DS}\}}$ and the estimation error reduction $\Delta\boldsymbol{\varepsilon}_{\boldsymbol{c}}$ of DS compared to AP are depicted in the left, middle and right column, respectively. The values in parentheses determine the required DS power overhead per pilot symbol compared to the data symbols $a_{m,k}$.

TABLE II
APPROXIMATED SIGNAL-TO-NOISE RATIO (SNR) VALUES IN ADDITIVE WHITE GAUSSIAN NOISE (AWGN) AND RAYLEIGH CHANNELS AND THE RELATED UNCODED BERS REQUIRED FOR > 90% THROUGHPUT FOR CERTAIN LTE MCSS ACCORDING TO [42]

M-QAM	MCS	SNR [dB] (AWGN)	BER (uncoded)	SNR [dB] (Rayleigh)
4	1-7	-5.5 to 5	0.3 to $3.75 \cdot 10^{-2}$	-4.1 to 10.7
16	8-10	7 to 11.5	0.12 to $3.45 \cdot 10^{-2}$	10 to 17
64	11-13	14 to 17	0.1 to $5.2 \cdot 10^{-2}$	17.2 to 21.2

d_Λ and the spreading matrix $\underline{C}$, the increase in channel estimation error is in line with the SIR of the data symbols shown in Figure 1. Similar to the AP scheme, the overall channel estimation performance $\varepsilon_H^{\{\mathrm{DS}\}}$ of the DS scheme is severely limited, as it is bounded by $\varepsilon_r^{\{\mathrm{DS}\}}$ (see left and right columns of Figure 6). For isotropic PFFs, i.e. EGF with $\alpha = 2$ and Hermite, the DS scheme can deliver a minimum $\varepsilon_H^{\{\mathrm{DS}\}}$ of approximately -18 dB. For non-isotropic PFFs, i.e. PHYDYAS and EGF $\alpha = 3$, $R_{\tilde{m},\tilde{k}}$ leads to an increase of the total estimation error to -11 dB and -14 dB. Additionally, the transmit power is increased. Compared to CP-OFDM the pilot pair ($p_{m,k}$ and $\rho_{m,k}$) has an average power rise of about -5.5 to 5.5 dB, which is significantly less than the power overhead of the AP scheme. The high value for the EGF PFF with $\alpha = 3$ can be reduced by a proper design of $\underline{\beta}$ and $\underline{C}$. For all PFFs, the channel estimation performance is limited by the residual estimation error $\varepsilon_r^{\{\mathrm{DS}\}}$ in the region of $\tau_{\mathrm{rms}}/T \leq 9 \cdot 10^{-3}$ and $f_D T \leq 3 \cdot 10^{-2}$. This may be improved by increasing the set $\mathbb{S}_C$ as proposed in [23], [24].

Comparing the AP and DS schemes, i.e. considering $\Delta\varepsilon_c$, depending on the applied pulse shape the DS scheme offers a superior channel estimation performance compared to the AP scheme with 2 to 3.5 dB gain as depicted in Figure 6c, 6f, 6i and 6l. However, simulations proved that due to the presence of $R_{\tilde{m},\tilde{k}}$, $\Delta\varepsilon_H = 0$ dB for approximately $\tau_{\mathrm{rms}}/T \leq 9 \cdot 10^{-3}$ and $f_D T \leq 3 \cdot 10^{-2}$. Outside this region the performance gain of the DS scheme is limited to 0.5 to 2 dB ($-\Delta\varepsilon_H$).

V. SYSTEM PERFORMANCE

In this section, the influence of the channel estimation error on the system level performance of the AP and DS schemes is evaluated. For this purpose, we consider a subset of the LTE scenarios depicted in Figure 1 and determine a suitable modulation scheme based on the achievable SIR and ε_H. The modulation scheme is obtained by defining a maximum threshold in terms of uncoded BER, from which the required minimum SNR SNR_{min} can be derived as reported in [43]. Finally, we can specify the minimum SIR $SIR_{d,\mathrm{min}}$ and the maximum channel estimation error $\varepsilon_{H,\mathrm{max}}$ required for data symbols approximately as follows:

$$SIR_{d,\mathrm{min}} \approx SNR_{\mathrm{min}} \tag{46a}$$

$$\varepsilon_{H,\mathrm{max}} \cong 2\frac{1}{1 + SNR_{\mathrm{min}}}. \tag{46b}$$

Although (46b) has been derived for the Minimum Mean-Squared Error (MMSE) estimator [44], it can serve as an upper performance bound for the LS estimation. The factor of two is introduced as parts of the estimation error do not affect the OQAM data symbols, since only the real part of demodulated symbols is taken into account. Based on the performance curves obtained for different Modulation and Coding Schemes (MCSs) provided in [42] for AWGN channels along with the corresponding uncoded BER values given in Table II, we consider a target uncoded BER of $5 \cdot 10^{-2}$ and obtain $SIR_{d,\mathrm{min}}$ and $\varepsilon_{H,\mathrm{max}}$ as shown in Table III.

Based on the channel scenarios presented in Table IV, Figures 7a, 7b and 7c as well as 7g, 7h and 7i depict a comparison of ε_H values, which are obtained analytically and via Monte-Carlo simulations for $K = 256$. For both interference mitigation schemes the results obtained

TABLE III
APPROXIMATED MINIMUM SNR SNR_{min} VALUES FOR A TARGET UNCODED BER OF $\leq 5 \cdot 10^{-2}$ FOR AN LTE SYSTEM OPERATING IN A RAYLEIGH CHANNEL AND RELATED VALUES FOR $SIR_{d,\mathrm{min}}$ AND $\varepsilon_{H,\mathrm{MAX}}$

M-QAM	SNR_{min} [dB]	$SIR_{d,\mathrm{min}}$ [dB]	$\varepsilon_{H,\mathrm{max}}$ [dB]
4	9.3	9.3	-6.8
16	15.1	15.1	-12.2
64	21.5	21.5	-18.53
256	28.2	28.2	-25.21
1024	35.2	35.2	-32.2

TABLE IV
SELECTED SCENARIOS FOR THE PERFORMANCE EVALUATION AT 800 MHZ CARRIER FREQUENCY INCLUDING THE THEORETICALLY OBTAINED M-QAM BASED ON THE APPROXIMATED $SIR_{d,\mathrm{min}}$ AS WELL AS THE APPLIED M-QUADRATURE AMPLITUDE MODULATION (QAM) LIMITED BY THE CHANNEL ESTIMATION ERROR $\varepsilon_{H,\mathrm{MAX}}$.

Name	Channel	$SIR_{d,\mathrm{min}}$ [dB]	M	$\varepsilon_{H,\mathrm{max}}$ [dB]	M
A	Tux 3 km/h	34	1024	-11 to -18	64
B	Rax 120 km/h	42.5	4096	-11 to -19	64
C	HTx 120 km/h	17.5	16	-9 to -11	16

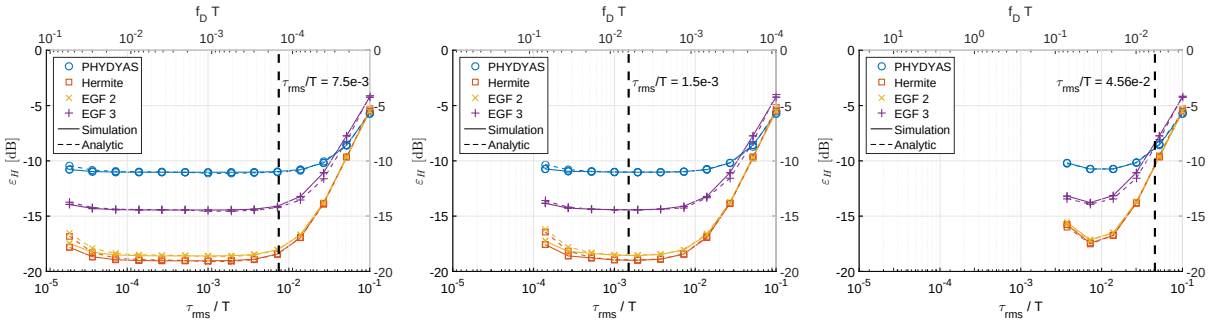

(a) $\boldsymbol{\varepsilon}_{\boldsymbol{H}}^{\{\mathrm{AP}\}}$ for scenario A (b) $\boldsymbol{\varepsilon}_{\boldsymbol{H}}^{\{\mathrm{AP}\}}$ for scenario B (c) $\boldsymbol{\varepsilon}_{\boldsymbol{H}}^{\{\mathrm{AP}\}}$ for scenario C

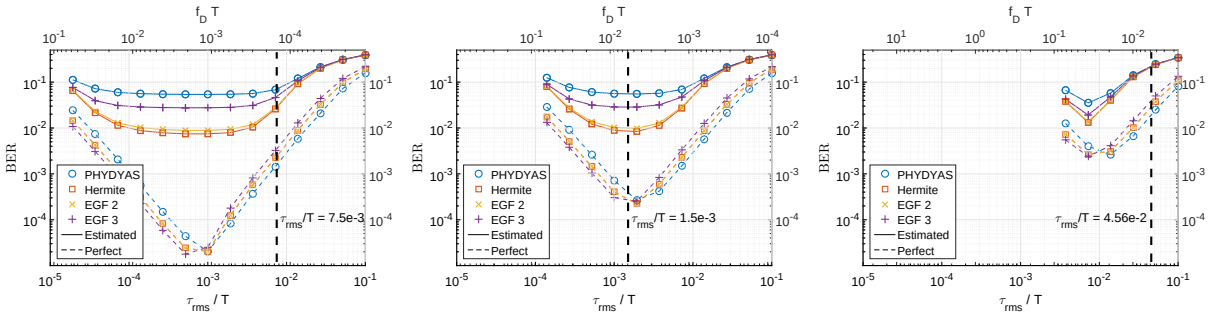

(d) BER for AP scheme in scenario A (e) BER for AP scheme in scenario B (f) BER for AP scheme in scenario C

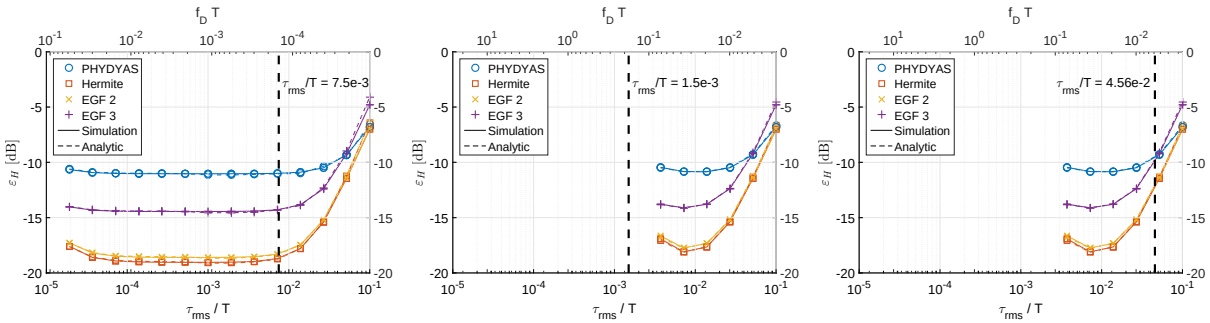

(g) $\boldsymbol{\varepsilon}_{\boldsymbol{H}}^{\{\mathrm{DS}\}}$ for scenario A (h) $\boldsymbol{\varepsilon}_{\boldsymbol{H}}^{\{\mathrm{DS}\}}$ for scenario B (i) $\boldsymbol{\varepsilon}_{\boldsymbol{H}}^{\{\mathrm{DS}\}}$ for scenario C

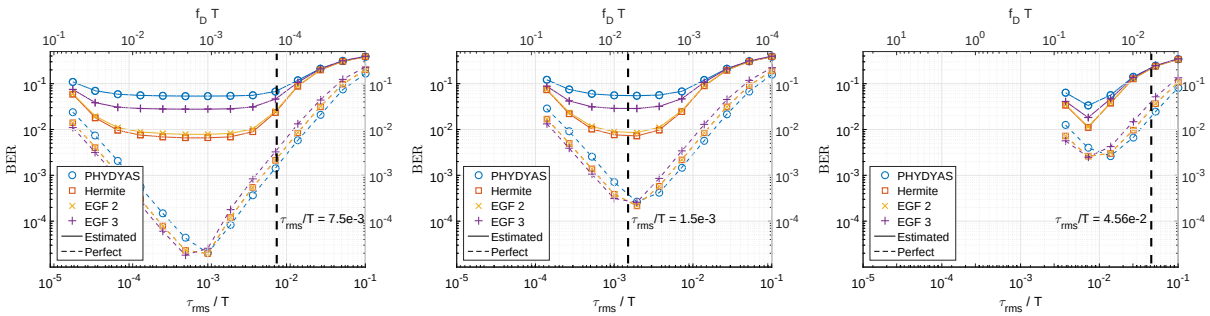

(j) BER for DS scheme in scenario A (k) BER for DS scheme in scenario B (l) BER for DS scheme in scenario C

Fig. 7. Channel estimation error for FBMC-OQAM systems, with $K = 256$ subcarriers and $\gamma = 4$, utilizing scattered pilots with pilot boost factor $b = 1$ operating in channel scenarios A to C according to Table IV. The dashed verticals indicate the equivalent normalized delay spread and maximum Doppler shift for the LTE subcarrier spacing, respectively.

analytically are in line with those based on simulations. They were carried out for $2 \cdot 10^3$ channel realizations, each having $5 \cdot 10^3$ transmitted FBMC-OQAM symbols. To avoid undersampling the channel impulse response and transfer function for high delay and Doppler spreads as well as to avoid interference between adjacent pilot symbols, the pilot symbols are placed in a checker pattern at every 8^{th} subcarrier and OQAM symbol, such that $2 \cdot 10^5$ pilot symbols are evaluated per channel realization. In order to equalize the data symbols, we apply a two-dimensional linear interpolation of the time-variant channel transfer function. The resulting uncoded BER values are depicted in 7d, 7e and 7f for the AP scheme as well as 7j, 7k and 7l for the DS scheme. It can be seen, that channel estimation based on the LS method results in a significant loss of BER performance of more than one order of magnitude.

In all considered scenarios, the residual interference on pilot symbols and thus MSE of the LS channel estimation is minimized for isotropic PFFs. Therefore, for these scenarios with the considered system design, CAPS cannot provide the uncoded BER performance gains of a factor of ≥ 2 as predicted by former studies [13]. However, CASS can provide performance enhancements for the scenarios A and C, where the LTE subcarrier spacing is not optimally matched to the channel characteristics. Besides the previous results, both investigated interference mitigation schemes are still able to reach the BER performance levels required by LTE. To support higher order modulation schemes, e.g. 256-QAM in LTE Advanced (Rel. 12), further improvements in the system design need to be found. Without increasing the receiver complexity, the channel estimation error and the related system performance can be improved by using boosted pilots ($b > 1$) or by reducing the residual estimation error by consideration of a higher number of neighboring symbols. Unfortunately, this in turn results in higher system complexity and might increase latency [24], [41].

VI. Conclusion and Outline

In this work we investigated the practical feasibility of FBMC-OQAM systems with CAM utilizing LS channel estimation based on the scattered pilot approach. Concerning this, analytical descriptions of interference mitigation based on the AP and DS schemes have been derived and evaluated. The resulting outcomes have been compared with Monte-Carlo based simulation results and a system level performance evaluation has been performed on the basis of uncoded BER. The results confirm, that for the specified system design, CAPS is subject to shortcomings concerning the residual channel estimation error, whereby isotropic PFFs show the best performance for each considered scenario. On the other hand, CASS provides significant performance gains and thus is seen as a promising concept for future system designs. Comparing the AP and DS schemes, DS provides a slightly better BER and ε_H performance in combination with a smaller pilot power increase of approximately 4 to 11 dB at the costs of higher computational complexity. The results showed that the DS scheme and the follow-up developments (e.g. [23], [24]) make scattered pilots a suitable approach for channel estimation in future communication systems.

In the future, we will investigate further interference mitigation schemes, e.g. POP methods [26], [27], as well as the performance improvements provided by pilot power boosting. Additionally, the effects of the amount of symbols considered for interference mitigation and the knowledge of the channel characteristics at the transmitter on the channel estimation performance will be investigated. Furthermore a trade-off analysis between the spectral efficiency loss caused by guard bands and the efficiency gain for a multi-user CAM or CASS scenario is subject of our future studies.

Acknowledgment

The authors would like to thank Malte Schellmann from Huawei European Research Center, Munich for fruitful discussions on aspects of this work.

Appendix A
Pilot Modulation Scheme for Channel Estimation Error Minimization

In (24), the pilot symbol $p_{\tilde{m},\tilde{k}}$ is statistically independent of $a_{\tilde{m}+\mu,\tilde{k}+\kappa}$ and $H_{\tilde{m},\tilde{k}}(\mu,\kappa)$. Therefore, $\varepsilon_H^{\{\text{AP}\}}$ can be expressed by

$$\varepsilon_H^{\{\text{AP}\}} = \mathbf{E}\left[|\tilde{p}_{\tilde{m},\tilde{k}}|^2\right] \mathbf{E}\left[\frac{1}{|p_{\tilde{m},\tilde{k}}|^2}\right], \tag{47}$$

with

$$\begin{aligned}\tilde{p}_{\tilde{m},\tilde{k}} = &\sum_{(\mu,\kappa)\in\mathbb{S}_R} \theta_{\mu,\kappa} a_{\tilde{m}+\mu,\tilde{k}+\kappa} H_{\tilde{m},\tilde{k}}(\mu,\kappa) \\ &+ \sum_{(\mu,\kappa)\in\mathbb{S}_C} \theta_{\mu,\kappa} a_{\tilde{m}+\mu,\tilde{k}+\kappa} \hat{H}(\mu,\kappa).\end{aligned} \tag{48}$$

Applying Jensen's inequality for convex functions, (47) can be written as

$$\varepsilon_H^{\{\text{AP}\}} \geq \frac{\mathbf{E}\left[|\tilde{p}_{\tilde{m},\tilde{k}}|^2\right]}{\mathbf{E}\left[|p_{\tilde{m},\tilde{k}}|^2\right]}. \tag{49}$$

Having this in regard, $\varepsilon_H^{\{\text{AP}\}}$ is minimized if

$$\mathbf{E}\left[\frac{1}{|p_{\tilde{m},\tilde{k}}|^2}\right] \equiv \frac{1}{\mathbf{E}\left[|p_{\tilde{m},\tilde{k}}|^2\right]}. \tag{50}$$

This is only fulfilled for $|p_{\tilde{m},\tilde{k}}| = \text{const.}$, such as for Binary Phase-Shift Keying (BPSK) modulated pilots. Accordingly, (24) yields

$$\varepsilon_H = \frac{1}{\sigma_p^2}\mathbf{E}\left[\left|\tilde{p}_{\tilde{m},\tilde{k}}\right|^2\right]. \tag{51}$$

Appendix B
Mean Interference Power of Received Symbol

Considering (9), the mean energy σ_I^2 of $\tilde{a}_{\tilde{m},\tilde{k}}^{\{I\}}$ is given by

$$\sigma_I^2 = \mathbf{E}\Bigg[\Bigg(\sum_{(\mu,\kappa)\in\mathbb{S}_N}\theta_{\mu,\kappa}a_{\tilde{m}+\mu,\tilde{k}+\kappa}H_{\tilde{m},\tilde{k}}(\mu,\kappa)\Bigg) \cdot\Bigg(\sum_{(\mu',\kappa')\in\mathbb{S}_N}\theta_{\mu',\kappa'}\tilde{a}_{\tilde{m},\tilde{k}}H_{\tilde{m},\tilde{k}}(\mu',\kappa')\Bigg)^*\Bigg]. \tag{52}$$

Performing the multiplication in consideration of statistical independence of $H_{\tilde{m},\tilde{k}}(\mu,\kappa)$ and $a_{\tilde{m}+\mu,\tilde{k}+\kappa}$, we obtain

$$\sigma_I^2 = \sum_{(\mu,\kappa)\in\mathbb{S}_N}\sum_{(\mu',\kappa')\in\mathbb{S}_N}\theta_{\mu,\kappa}\theta_{\mu',\kappa'}^*\mathbf{E}\left[a_{\tilde{m}+\mu,\tilde{k}+\kappa}a_{\tilde{m}+\mu',\tilde{k}+\kappa'}^*\right] \cdot\underbrace{\mathbf{E}\left[H_{\tilde{m},\tilde{k}}(\mu,\kappa)H_{\tilde{m},\tilde{k}}^*(\mu',\kappa')\right]}_{\sigma_{\mu,\mu'}^{\kappa,\kappa'}(\tilde{k})}, \tag{53}$$

with $\sigma_{\mu,\mu'}^{\kappa,\kappa'}(\tilde{k})$ being the cross-correlation of any combination of $H_{\tilde{m},\tilde{k}}(\mu,\kappa)$ and $H_{\tilde{m},\tilde{k}}^*(\mu',\kappa')$. Recalling (10), $\sigma_{\mu,\mu'}^{\kappa,\kappa'}(\tilde{k})$ can be written as

$$\sigma_{\mu,\mu'}^{\kappa,\kappa'}(\tilde{k}) = \sum_{l=0}^{L-1}\sum_{l'=0}^{L-1}\int_{-f_D}^{f_D}\int_{-f_D}^{f_D}\mathbf{E}\left[h_D[\tau_l,\nu]h_D^*[\tau_{l'},\nu']\right] \cdot A_{\mu,\kappa}^{\tilde{k}}[\tau_l,\nu]\left(A_{\mu',\kappa'}^{\tilde{k}}[\tau_{l'},\nu']\right)^*\mathrm{d}\nu\,\mathrm{d}\nu'. \tag{54}$$

From the Wide Sense Stationary (WSS) Uncorrelated Scattering (US) condition of the propagation channel, $\mathbf{E}\left[h_D[\tau_l,\nu]h_D^*[\tau_{l'},\nu']\right] = g_l D(\nu)\delta_{l,l'}\delta_{\nu,\nu'}$ follows and (54) yields

$$\sigma_{\mu,\mu'}^{\kappa,\kappa'}(\tilde{k}) = \sum_{l=0}^{L-1}\int_{-f_D}^{f_D} g_l D(\nu)A_{\mu,\kappa}^{\tilde{k}}[\tau_l,\nu]\left(A_{\mu',\kappa'}^{\tilde{k}}[\tau_{l'},\nu']\right)^*\mathrm{d}\nu. \tag{55}$$

It should be noticed that a term in (53) is only zero in case the modulated symbols are i.i.d., i.e. $\mathbf{E}\left[a_{\tilde{m}+\mu,\tilde{k}+\kappa}a_{\tilde{m}+\mu',\tilde{k}+\kappa'}^* = \sigma_a^2\delta_{\mu,\mu'}\delta_{\kappa,\kappa'}\right]$, which is not guaranteed for all interference mitigation schemes investigated in this contribution. With $a_{m,k}$ being i.i.d., (53) can be written as

$$\sigma_I^2 = \sigma_a^2\sum_{(\mu,\kappa)\in\mathbb{S}_N}\sum_{l=0}^{L-1}\int_{-f_D}^{f_D} g_l D(\nu)\left|A_{\mu,\kappa}[\tau_l,\nu]\right|^2\mathrm{d}\nu. \tag{56}$$

Appendix C
Channel Estimation Error for DS Scheme

Similar to appendix B, the mean square error $\varepsilon_H^{\{\mathrm{DS}\}}$ is defined by

$$\begin{aligned}\varepsilon_H^{\{\mathrm{DS}\}} &= \mathbf{E}\Bigg[\Bigg|\sum_{(\mu,\kappa)\in\mathbb{S}_R}\theta_{\mu,\kappa}^*\frac{a_{\tilde{m}+\mu,\tilde{k}+\kappa}}{p_{\tilde{m},\tilde{k}}}H_{\tilde{m},\tilde{k}}(\mu,\kappa) + \sum_{\lambda=1}^{\Lambda}H_\lambda\frac{\underline{\chi}_\lambda\underline{d}}{p_{\tilde{m},\tilde{k}}}\Bigg|^2\Bigg] \\ &= \mathbf{E}\Bigg[\Bigg(\sum_{(\mu,\kappa)\in\mathbb{S}_R}\theta_{\mu,\kappa}^*\frac{a_{\tilde{m}+\mu,\tilde{k}+\kappa}}{p_{\tilde{m},\tilde{k}}}H_{\tilde{m},\tilde{k}}(\mu,\kappa) + \sum_{\lambda=1}^{\Lambda}H_\lambda\frac{\underline{\chi}_\lambda\underline{d}}{p_{\tilde{m},\tilde{k}}}\Bigg) \cdot\Bigg(\sum_{(\mu',\kappa')\in\mathbb{S}_R}\theta_{\mu',\kappa'}^*\frac{a_{\tilde{m}+\mu',\tilde{k}+\kappa'}}{p_{\tilde{m},\tilde{k}}}H_{\tilde{m},\tilde{k}}(\mu',\kappa') + \sum_{\lambda'=1}^{\Lambda}H_{\lambda'}\frac{\underline{\chi}_{\lambda'}\underline{d}}{p_{\tilde{m},\tilde{k}}}\Bigg)^*\Bigg].\end{aligned} \tag{57}$$

Considering appendix A and with the assumption of i.i.d. data symbols, i.e. $\mathbf{E}\left[a_{\tilde{m}+\mu,\tilde{k}+\kappa}a_\lambda^*\right] = 0$ and $\mathbf{E}\left[a_{\tilde{m}+\mu,\tilde{k}+\kappa}a_{\tilde{m}+\mu',\tilde{k}+\kappa'}^*\right] = \sigma_d^2\delta_{\mu,\mu'}\delta_{\kappa,\kappa'}$, pilot boost factor $b = \sigma_p^2/\sigma_d^2$ and BPSK modulated pilot symbols, (57) can be simplified as

$$\varepsilon_H^{\{\mathrm{DS}\}} = \varepsilon_c^{\{\mathrm{DS}\}} + \varepsilon_r^{\{\mathrm{DS}\}} \tag{58}$$

with

$$\begin{aligned}\varepsilon_c^{\{\mathrm{DS}\}} &= \frac{1}{\sigma_p^2}\sum_{(\lambda,\lambda')}\mathbf{E}\left[H_\lambda H_{\lambda'}^*\right]\mathbf{E}\left[a_\lambda a_{\lambda'}^*\right] \\ &= \frac{1}{\sigma_p^2}\sum_{(\lambda,\lambda')}\mathbf{E}\left[H_\lambda H_{\lambda'}^*\right]\underline{\chi}_\lambda\mathbf{E}\left[\underline{d}\,\underline{d}^H\right]\underline{\chi}_{\lambda'}^T\end{aligned} \tag{59}$$

and

$$\begin{aligned}\varepsilon_r^{\{\mathrm{DS}\}} &= \frac{1}{b}\sum_{(\mu,\kappa)\in\mathbb{S}_R}\mathbf{E}\left[\left|H_{\tilde{m},\tilde{k}}(\mu,\kappa)\right|^2\right] \\ &= \varepsilon_r^{\{\mathrm{AP}\}}.\end{aligned} \tag{60}$$

Taking into account that

$$\mathbf{E}\left[d_\lambda d_{\lambda'}^*\right] = \begin{cases}\sigma_d^2, & \lambda = \lambda' \neq \Lambda \\ \sigma_d^2\sigma_\beta^2 & \lambda = \lambda' = \Lambda \\ \sigma_d^2\beta_{\lambda'} & \lambda \neq \Lambda \wedge \lambda' = \Lambda \\ \sigma_d^2\beta_\lambda & \lambda = \Lambda \wedge \lambda' \neq \Lambda \\ 0 & \text{otherwise}\end{cases}, \tag{61}$$

the cancellation error $\varepsilon_c^{\{\mathrm{DS}\}}$ yields

$$\begin{aligned}\varepsilon_c^{\{\mathrm{DS}\}} =& \frac{1}{b}\sum_{(\lambda,\lambda')} \mathbf{E}\left[H_\lambda H_{\lambda'}^*\right] \underline{\chi}_\lambda \underline{B}_I \underline{\chi}_{\lambda'}^T \\ =& \frac{1}{b}\sum_{(\lambda,\lambda')} \mathbf{E}\left[H_\lambda H_{\lambda'}^*\right] \left(\delta_{\lambda,\lambda'} + \underline{\chi}_\lambda \underline{B} \underline{\chi}_{\lambda'}^T\right) \\ =& \frac{1}{b}\sum_{\lambda} \mathbf{E}\left[|H_\lambda|^2\right] + \frac{1}{b}\sum_{(\lambda,\lambda')} \mathbf{E}\left[H_\lambda H_{\lambda'}^*\right] \left(\underline{\chi}_\lambda \underline{B} \underline{\chi}_{\lambda'}^T\right),\end{aligned} \tag{62}$$

with $\underline{B}_I$ and $\underline{B}$ being correlation matrices defined by

$$\begin{aligned}\underline{B}_I &= \begin{bmatrix} \underline{I}_{\Lambda-1} & \underline{\beta}^T \\ \underline{\beta} & \sigma_\beta^2 \end{bmatrix} \\ &= \underline{I}_\Lambda + \underline{B} = \underline{I}_\Lambda + \begin{bmatrix} \underline{O}_{\Lambda-1} & \underline{\beta}^T \\ \underline{\beta} & \sigma_\beta^2 - 1 \end{bmatrix}.\end{aligned} \tag{63}$$

Here, $\underline{I}_{\Lambda-1}$ and $\underline{O}_{\Lambda-1}$ are the identity and zero matrix of size $\Lambda-1$, respectively. As both $\varepsilon_c^{\{\mathrm{DS}\}}$ and $\varepsilon_r^{\{\mathrm{DS}\}}$ include a term for the full interference induced by a symbol, $\varepsilon_H^{\{\mathrm{DS}\}}$ can be rewritten as

$$\begin{aligned}\varepsilon_H^{\{\mathrm{DS}\}} =& \frac{1}{b}\sum_{(\mu,\kappa)\in\mathbb{S}_N} \mathbf{E}\left[|H_{\tilde{m},\tilde{k}}(\mu,\kappa)|^2\right] \\ &+ \frac{1}{b}\sum_{(\lambda,\lambda')} \mathbf{E}\left[H_\lambda H_{\lambda'}^*\right] \left(\underline{\chi}_\lambda \underline{B} \underline{\chi}_{\lambda'}^T\right).\end{aligned} \tag{64}$$

Utilizing (55) results in

$$\begin{aligned}\varepsilon_H^{\{\mathrm{DS}\}} =& \frac{1}{b}\sum_{l=0}^{L-1}\int_{-f_D}^{f_D} g_l D(\nu)\Bigg(\sum_{(\mu,\kappa)\in\mathbb{S}_N} |A_{\mu,\kappa}[\tau_l,\nu]|^2 \\ &+ \sum_{(\lambda,\lambda')} \Big(\theta_{(\mu,\kappa)_\lambda} A_{(\mu,\kappa)_\lambda}[\tau_l,\nu] x_{\lambda,\lambda'} \\ &\cdot \theta^*_{(\mu,\kappa)_{\lambda'}} A^*_{(\mu,\kappa)_{\lambda'}}[\tau_l,\nu]\Big)\Bigg)\mathrm{d}\nu \\ =& \frac{1}{b}\sum_{l=0}^{L-1}\int_{-f_D}^{f_D} g_l D(\nu) \\ &\cdot \left(\sum_{(\mu,\kappa)\in\mathbb{S}_N} |A_{\mu,\kappa}[\tau_l,\nu]|^2 + \underline{\alpha}_{\tau_l,\nu} \underline{X}\, \underline{\alpha}_{\tau_l,\nu}^H\right)\mathrm{d}\nu\end{aligned} \tag{65}$$

with $x_{\lambda,\lambda'}$, $\underline{X}$ and $\underline{\alpha}_{\tau_l,\nu}$ being defined according to

$$x_{\lambda,\lambda'} = \underline{\chi}_\lambda \underline{B} \underline{\chi}_{\lambda'}^T \tag{66a}$$

$$\underline{\alpha}_{\tau_l,\nu} = \left[\theta_{(\mu,\kappa)_1} A_{(\mu,\kappa)_1}[\tau_l,\nu], \ldots, \theta_{(\mu,\kappa)_\Lambda} A_{(\mu,\kappa)_\Lambda}[\tau_l,\nu]\right]^T \tag{66b}$$

$$\begin{aligned}\underline{X} = \underline{X}^T =& \underline{C}\,\underline{B}\,\underline{C}^T \\ =& \begin{bmatrix} x_{1,1} & \ldots & x_{1,\lambda'} & \ldots & x_{1,\Lambda} \\ \vdots & \ddots & \vdots & \ddots & \vdots \\ x_{\lambda,1} & \ldots & x_{\lambda,\lambda'} & \ldots & x_{\lambda,\Lambda} \\ \vdots & \ddots & \vdots & \ddots & \vdots \\ x_{\Lambda,1} & \ldots & x_{\Lambda,\lambda'} & \ldots & x_{\Lambda,\Lambda} \end{bmatrix}.\end{aligned} \tag{66c}$$

Similar to the AP scheme, the phase shifted discrete-time ambiguity function can be substituted by the discrete-time ambiguity function, as the phase shifts are canceled out in $\underline{\alpha}_{\tau_l,\nu} \underline{X}\, \underline{\alpha}_{\tau_l,\nu}^H$ (without proof).

Appendix D
DS Scheme Matrices

In order of completeness, the spreading matrices $\underline{C}$ reported in [19] and the calculation of the auxiliary data symbols d_Λ and the variables β and $\underline{X}$ are outlined with the notation used in this work. For isotropic pulse shapes, $\underline{C}$ and d_Λ are defined according to

$$d_\Lambda = d_8 = -2\frac{-\mathrm{j}A_{1,1}[0,0]}{A_{0,1}[0,0] + A_{1,0}[0,0]} d_7 = \mathrm{j}\frac{A_{1,1}[0,0]}{A_{1,0}[0,0]} d_7 \tag{67}$$

$$\underline{C} = \frac{1}{2}\begin{bmatrix} 1 & 0 & 1 & 0 & 0 & 1 & 1 & 0 \\ 0 & 1 & 0 & 1 & 1 & 0 & 0 & -1 \\ 1 & 0 & -1 & 0 & 0 & -1 & 1 & 0 \\ 0 & 1 & 0 & -1 & -1 & 0 & 0 & -1 \\ 0 & 1 & 0 & 1 & -1 & 0 & 0 & 1 \\ -1 & 0 & 1 & 0 & 0 & -1 & 1 & 0 \\ 0 & 1 & 0 & -1 & 1 & 0 & 0 & 1 \\ -1 & 0 & -1 & 0 & 0 & 1 & 1 & 0 \end{bmatrix}. \tag{68}$$

From this, it follows that

$$\beta_\lambda = \begin{cases} \mathrm{j}\frac{A_{1,1}[0,0]}{A_{1,0}[0,0]}, & \lambda = 7 \\ 0, & \text{otherwise} \end{cases}. \tag{69}$$

Through this, $\underline{X}$ in (41) can be written as

$$\underline{X} = \frac{1}{4}\begin{bmatrix} \underline{X}_1 & \underline{X}_1 & \underline{X}_2 & \underline{X}_2 \\ \underline{X}_1 & \underline{X}_1 & \underline{X}_2 & \underline{X}_2 \\ \underline{X}_2^T & \underline{X}_2^T & \underline{R}^T\underline{X}_1\underline{R} & \underline{R}^T\underline{X}_1\underline{R} \\ \underline{X}_2^T & \underline{X}_2^T & \underline{R}^T\underline{X}_1\underline{R} & \underline{R}^T\underline{X}_1\underline{R} \end{bmatrix}, \tag{70}$$

where $\underline{X}_1$, $\underline{X}_2$ and the rotation matrix $\underline{R}$ are given by

$$\underline{X}_1 = \begin{bmatrix} 0 & -\beta_7 \\ -\beta_7 & \beta_7^2 - 1 \end{bmatrix} \tag{71a}$$

$$\underline{X}_2 = \begin{bmatrix} \beta_7 & 0 \\ -\beta_7^2 + 1 & -\beta_7 \end{bmatrix} \tag{71b}$$

$$\underline{R} = \begin{bmatrix} 0 & 1 \\ -1 & 0 \end{bmatrix}. \tag{71c}$$

For non-isotropic pulse shapes, $\underline{C}$ and d_Λ are defined according to

$$d_\Lambda = d_8 = \sqrt{2}\frac{-\mathrm{j}A_{1,1}[0,0]}{A_{1,0}[0,0]}d_5 - \frac{A_{0,1}[0,0]}{A_{1,0}[0,0]}d_7 \tag{72}$$

$$\underline{C} = \frac{1}{2}\begin{bmatrix} 1 & 0 & 1 & 0 & 1 & 1 & 0 & 0 \\ 0 & \sqrt{2} & 0 & 0 & 0 & 0 & -\sqrt{2} & 0 \\ 1 & 0 & -1 & 0 & 1 & -1 & 0 & 0 \\ 0 & 0 & 0 & \sqrt{2} & 0 & 0 & 0 & -\sqrt{2} \\ 0 & 0 & 0 & \sqrt{2} & 0 & 0 & 0 & \sqrt{2} \\ -1 & 0 & 1 & 0 & 1 & -1 & 0 & 0 \\ 0 & \sqrt{2} & 0 & 0 & 0 & 0 & \sqrt{2} & 0 \\ -1 & 0 & -1 & 0 & 1 & 1 & 0 & 0 \end{bmatrix}, \tag{73}$$

and subsequently,

$$\beta_\lambda = \begin{cases} -\mathrm{j}\sqrt{2}\frac{A_{1,1}[0,0]}{A_{1,0}[0,0]}, & \lambda = 5 \\ -\frac{A_{0,1}[0,0]}{A_{1,0}[0,0]}, & \lambda = 7 \\ 0, & \text{otherwise} \end{cases}. \tag{74}$$

Through this, $\underline{X}$ of (41) can be written as

$$\underline{X} = \frac{1}{4}\begin{bmatrix} \underline{O}_3 & \underline{X}_1^T & -\underline{X}_1^T & \underline{O}_3 \\ \underline{X}_1 & \chi & -\chi & -\underline{X}_2 \\ -\underline{X}_1 & -\chi & \chi & \underline{X}_2 \\ \underline{O}_3 & -\underline{X}_2^T & \underline{X}_2^T & \underline{O}_3 \end{bmatrix}, \tag{75}$$

where $\underline{X}_1$, $\underline{X}_2$ and χ are given by

$$\underline{X}_1 = \begin{bmatrix} -\sqrt{2}\beta_5 & 2\beta_7 & -\sqrt{2}\beta_5 \end{bmatrix} \tag{76a}$$

$$\underline{X}_2 = \begin{bmatrix} \sqrt{2}\beta_5 & 2\beta_7 & \sqrt{2}\beta_5 \end{bmatrix} \tag{76b}$$

$$\chi = 2(\beta_5^2 + \beta_7^2 - 1). \tag{76c}$$

References

[1] A. Osseiran, F. Boccardi, V. Braun, K. Kusume, P. Marsch, M. Maternia, O. Queseth, M. Schellmann, H. Schotten, H. Taoka, H. Tullberg, M. A. Uusitalo, B. Timus, and M. Fallgren, "Scenarios for 5G mobile and wireless communications: the vision of the METIS project," *IEEE Commun. Mag.*, vol. 52, no. 5, pp. 26–35, may 2014.

[2] 3GPP TS 36.201, "LTE physical layer; General description (Release 9)," 3GPP TSG RAN, Tech. Rep. v9.1.0, 2010.

[3] B. Le Floch, M. Alard, and C. Berrou, "Coded orthogonal frequency division multiplex [TV broadcasting]," *Proc. IEEE*, vol. 83, no. 6, pp. 982–996, jun 1995.

[4] V. Vakilian, T. Wild, F. Schaich, S. ten Brink, and J.-F. Frigon, "Universal-filtered multi-carrier technique for wireless systems beyond LTE," in *2013 IEEE Globecom Work. (GC Wkshps)*. Atlanta, GA, USA: IEEE, dec 2013, pp. 223–228.

[5] P. Siohan, C. Siclet, and N. Lacaille, "Analysis and design of OFDM/OQAM systems based on filterbank theory," *IEEE Trans. Signal Process.*, vol. 50, no. 5, pp. 1170–1183, may 2002.

[6] M. Schellmann, Z. Zhao, H. Lin, P. Siohan, N. Rajatheva, V. Luecken, and A. Ishaque, "FBMC-based air interface for 5G mobile: Challenges and proposed solutions," in *Proc. 9th Int. Conf. Cogn. Radio Oriented Wirel. Networks*, no. i. ICST, 2014, pp. 102 – 107.

[7] S. E. El Ayoubi, M. Boldi, Ö. Bulakci, P. Spapis, M. Schellmann, P. Marsch, M. Säily, J. F. Monserrat, T. Rosowski, G. Zimmermann, I. D. Silva, M. Tesanovic, M. Shariat, and Ahmed M. Ibrahim, "Preliminary views and initial considerations on 5G RAN architecture and functional design," *White Pap. METIS II*, pp. 1–27, 2016.

[8] A. Viholainen, M. Bellanger, and M. Huchard, "Prototype filter and structure optimization," EU Project, Tech. Rep. ICT-211887 PHYDYAS Deliverable D5.1, 2009.

[9] M. Gharba, R. Legouable, and P. Siohan, "An alternative multiple access scheme for the uplink 3GPP/LTE based on OFDM/OQAM," in *2010 7th Int. Symp. Wirel. Commun. Syst.* IEEE, sep 2010, pp. 941–945.

[10] F. Schaich, J. Vandermot, V. Ringset, H. Rustad, M. Najar, F. Rubio, M. Caus, and Z. Zhipeng, "WiMAX simulation results - Lab setup and measurements," EU Project, Tech. Rep. ICT-211887 PHYDYAS Deliverable D9.3, 2010.

[11] T. Strohmer and S. Beaver, "Optimal OFDM design for time-frequency dispersive channels," *IEEE Trans. Commun.*, vol. 51, no. 7, pp. 1111–1122, jul 2003.

[12] H. Lin and P. Siohan, "Robust channel estimation for OFDM/OQAM," *IEEE Commun. Lett.*, vol. 13, no. 10, pp. 724–726, oct 2009.

[13] M. Fuhrwerk, J. Peissig, and M. Schellmann, "Channel adaptive pulse shaping for OQAM-OFDM systems," in *2014 22nd Eur. Signal Process. Conf.*, sep 2014, pp. 181–185.

[14] J. Du and S. Signell, "Pulse shape adaptivity in OFDM/OQAM systems," in *Proc. 2008 Int. Conf. Adv. Infocomm Technol. - ICAIT '08*. New York, New York, USA: ACM Press, 2008, pp. 1–5.

[15] M. Fuhrwerk, J. Peissig, and M. Schellmann, "Performance comparison of CP-OFDM and OQAM-OFDM systems based on LTE parameters," in *2014 IEEE 10th Int. Conf. Wirel. Mob. Comput. Netw. Commun.* IEEE, oct 2014, pp. 604–610.

[16] M. Failli, "Digital land mobile radio-communications," Commission of the European Communities, Tech. Rep. ICT COST Action 207, 1989.

[17] M. Fuhrwerk, J. Peissig, and M. Schellmann, "On the design of an FBMC based air interface enabling channel adaptive pulse shaping per sub-band," in *2015 23rd Eur. Signal Process. Conf.* IEEE, aug 2015, pp. 384–388.

[18] J.-P. Javaudin, D. Lacroix, and A. Rouxel, "Pilot-aided channel estimation for OFDM/OQAM," in *57th IEEE Semiannu. Veh. Technol. Conf. 2003. VTC 2003-Spring.*, vol. 3, no. 3. IEEE, 2003, pp. 1581–1585.

[19] C. Lélé, R. Legouable, and P. Siohan, "Channel estimation with scattered pilots in OFDM/OQAM," in *2008 IEEE 9th Work. Signal Process. Adv. Wirel. Commun.*, no. 2. IEEE, jul 2008, pp. 286–290.

[20] J. Bazzi, P. Weitkemper, and K. Kusume, "Power efficient scattered pilot channel estimation for FBMC/OQAM," in *SCC 2015; 10th Int. ITG Conf. Syst. Commun. Coding; Proc.* VDE, 2015, pp. 1–6.

[21] T. W. Yoon, S. B. Im, S. H. Hwang, and H. J. Choi, "Pilot structure for high data rate in OFDM/OQAM-IOTA system," in *2008 IEEE 68th Veh. Technol. Conf.* IEEE, sep 2008, pp. 1–5.

[22] X. Mestre and E. Kofidis, "Pilot-based channel estimation for FBMC/OQAM systems under strong frequency selectivity," in *2016 IEEE Int. Conf. Acoust. Speech Signal Process.* IEEE, mar 2016, pp. 3696–3700.

[23] W. Cui, D. Qu, T. Jiang, and B. Farhang-Boroujeny, "Coded auxiliary pilots for channel estimation in FBMC-OQAM systems," *IEEE Trans. Veh. Technol.*, vol. 65, no. 5, pp. 2936–2946, may 2016.

[24] R. Nissel and M. Rupp, "On pilot-symbol aided channel estimation in FBMC-OQAM," in *2016 IEEE Int. Conf. Acoust. Speech Signal Process.* IEEE, mar 2016, pp. 3681–3685.

[25] C. Lélé, "Iterative scattered-based channel estimation method for OFDM/OQAM," *EURASIP J. Adv. Signal Process.*, vol. 2012, no. 1, p. 42, 2012.

[26] C. Lélé, J.-P. Javaudin, R. Legouable, A. Skrzypczak, and P. Siohan, "Channel estimation methods for preamble-based OFDM/OQAM modulations," *Eur. Trans. Telecommun.*, vol. 19, no. 7, pp. 741–750, nov 2008.

[27] J.-M. Choi, Y. Oh, H. Lee, and J.-S. Seo, "Interference-dependent pair of pilots for channel estimation in FBMC systems," in *2016*

IEEE Int. Symp. Broadband Multimed. Syst. Broadcast. IEEE, jun 2016, pp. 1–4.

[28] Z. Zhao, N. Vucic, and M. Schellmann, "A simplified scattered pilot for FBMC/OQAM in highly frequency selective channels," in *2014 11th Int. Symp. Wirel. Commun. Syst.* IEEE, aug 2014, pp. 819–823.

[29] 3GPP TR 25.943, "Deployment aspects (Release 10)," 3GPP TSG RAN, Tech. Rep. V10.0.0, 2011.

[30] A. F. Molisch, *Wireless Communications*, 2nd ed. Wiley - IEEE, 2010.

[31] M. G. Bellanger, "Specification and design of a prototype filter for filter bank based multicarrier transmission," in *2001 IEEE Int. Conf. Acoust. Speech, Signal Process. Proc. (Cat. No.01CH37221)*, vol. 4. IEEE, 2001, pp. 2417–2420.

[32] P. Siohan and C. Roche, "Cosine-modulated filterbanks based on extended Gaussian functions," *IEEE Trans. Signal Process.*, vol. 48, no. 11, pp. 3052–3061, 2000.

[33] R. Haas and J.-C. Belfiore, "Multiple carrier transmission with time-frequency well-localized impulses," in *IEEE Second Symp. Commun. Veh. Technol. Benelux*, no. 2. Univ. Catholique de Louvain, 1994, pp. 187–193.

[34] W. Kozek and A. F. Molisch, "Nonorthogonal pulseshapes for multicarrier communications in doubly dispersive channels," *IEEE J. Sel. Areas Commun.*, vol. 16, no. 8, pp. 1579–1589, 1998.

[35] S. Mirabbasi and K. Martin, "Design of prototype filter for near-perfect-reconstruction overlapped complex-modulated transmultiplexers," in *2002 IEEE Int. Symp. Circuits Syst. Proc. (Cat. No.02CH37353)*, vol. 1. IEEE, 2002, pp. I–821–I–824.

[36] E. Kofidis, D. Katselis, A. Rontogiannis, and S. Theodoridis, "Preamble-based channel estimation in OFDM/OQAM systems: A review," *Signal Processing*, vol. 93, no. 7, pp. 2038–2054, jul 2013.

[37] E. Kofidis, "Channel estimation in filter bank-based multicarrier systems: Challenges and solutions," in *2014 6th Int. Symp. Commun. Control Signal Process.* IEEE, may 2014, pp. 453–456.

[38] T. Fusco, A. Petrella, and M. Tanda, "Data-aided symbol timing and CFO synchronization for filter bank multicarrier systems," *IEEE Trans. Wirel. Commun.*, vol. 8, no. 5, pp. 2705–2715, may 2009.

[39] T. H. Stitz, T. Ihalainen, A. Viholainen, and M. Renfors, "Pilot-based synchronization and equalization in filter bank multicarrier communications," *EURASIP J. Adv. Signal Process.*, vol. 2010, pp. 1–19, 2010.

[40] C. Thein, M. Schellmann, and J. Peissig, "Analysis of frequency domain frame detection and synchronization in OQAM-OFDM systems," *EURASIP J. Adv. Signal Process.*, vol. 2014, no. 1, p. 83, 2014.

[41] Jérôme Louveaux, L. Baltar, D. Waldhauser, M. Renfors, M. Tanda, C. Bader, and E. Kofidis, "Equalization and demodulation in the receiver (single antenna)," EU Project, Tech. Rep. ICT-211887 PHYDYAS Deliverable D3.1, 2008.

[42] "Radio frequency (RF) system scenarios (Release 13)," 3GPP, Tech. Rep. TR 36.942 v13.0.0, 2016.

[43] M. K. Simon and M.-S. Alouini, *Digital Communication Over Fading Channels*. New York, USA: John Wiley & Sons, Inc., 2000.

[44] D. Guo, S. Shamai, and S. Verdú, "Mutual information and minimum mean-square error in Gaussian channels," *IEEE Trans. Inf. Theory*, vol. 51, no. 4, pp. 1261–1282, apr 2005.